وزارة التعليم العالي والبحث العلمي

BADJI MOKHTAR UNIVERSITY
ANNABA

جامعة باجي مختار – عنابة –

Faculty of Science

Department of Physics

DOCTORATE THESIS

(Physics of metallic materials)

By:
Aicha LOUCIF

Microstructural Evolution in an AlSiMg Alloy Subjected to Severe Plastic Deformation

Presented on June 27, 2012 front the Jury:

Prof. H. Meradji	Annaba University	President
Dr. R. Chemam	Annaba University	Supervisor
Prof. D. Bradai	USTHB University	Member
Prof. A. Saker	Annaba University	Member
Dr. R. Ayache	Batna University	Member
Dr. T. Baudin	Paris-Sud University	Member

Acknowledgements

I would like to express my deep sense of gratitude to my supervisor Dr. R. Chemam for his excellent supervision, invaluable suggestions and constant encouragement throughout my Ph.D duration. His relentless support, enthusiasm, wisdom and patience gave me all the zeal to push forward with my work.

I express my gratitude to Professor H. Meradji from Annaba University, for the honor given me to chair the jury.

I take this opportunity to thank Professor A. Saker, from Annaba University, Professor D. Bradai, from Bab Ezouar University, Dr. R. Ayache from Batna University and Dr. T. Baudin, for being part of the jury members.

I am grateful to Professor T. G. Langdon and Dr. T. Baudin, whose help has given the courage to begin my Ph.D, which is stepping stone to my success. Thank you for all your support, guidance, patience, hard work and rich discussions which were great help for me to make my work worth. I am very thankful to you for taking every effort from the beginning until the end of publishing the papers, for allowing me to carry out the project work and permitting the use of necessary facilities for successful completion of the work. Thank you whole-heartedly for endeavor you have taken to guide me and make the best of my work.

My sincere thanks to Dr R. B. Figueiredo for being patience and kind all through my work and made every effort to help me, yet uncounted and in making this work and to see the light of success. Thank you for your patience and for doing the HPT tests. I would also thank Dr. F. Brisset and Dr. M Kawasaki for their help in completing my work. I am thankful for the time you devoted to do the experimental procedure and helping me too.

Thanks to Professor B. Hanech for his encouragement for allowing me to do heat treatments in his laboratory. Thanks also to A. Garbi for his kind support in hardness measurement.

I take this privilege to extend my thanks and gratitude towards all the members of the laboratory LPR. I would also like to thank all my friends who have assisted me at all moments of need. Finally, I thank all personalities who either directly or indirectly rendered help to complete the project work successfully.

I express my profound gratitude to my family for their sacrifices, constant support, understanding and encouragement extended.

Résume

Le présent travail vise à révéler l'évolution de la microstructure et le comportement mécanique d'un alliage d'aluminium commercial Al-0.6% Mg-0.4% Si soumis à une déformation plastique sévère. La déformation plastique a été réalisée à l'aide d'une torsion sous haute pression (HPT) effectuée sous une pression de 6.0 GPa. Avant la déformation, les disques ont subi un traitement d'homogénéisation à 813 K pendant 2h suivis d'un vieillissement pendant une courte durée de 5 minutes à des température de 473 K et 523 K. Les disques après mise en solution et vieillis ont subi jusqu'à 20 tours de torsion. L'évolution des microstructures, des microtextures ainsi que des propriétés mécaniques des disques dans ces trois conditions a été suivie par le biais d'une analyse par diffraction des électrons rétrodiffusés (EBSD), d'essais microdureté et de traction. Un affinement prononcé des grains est obtenue après seulement une tour de torsion. La taille moyenne atteint environ 250 nm après 20 tours ce qui traduit par une augmentation de la dureté qui tend à saturer déformations équivalentes de l'ordre de 100. La fraction de joints de grains à grande angles de désorientation augmente avec la déformation. Une corrélation entre l'évolution de la dureté et la taille des grains semble obéir à la loi conventionnelle de Hall-Petch pour les tailles des grains relativement importantes mais dévie sensiblement lorsque cette taille devient inférieur à 500 nm. Cette déviation a été expliquée par le fait que la loi de Hall-Petch semble ne plus s'appliquer à cause du mouvement des dislocations extrinsèques aux joints de grains en état de non équilibre thermodynamique. Les résultats des tests de traction, menées à la température de 813 K avec une vitesse de déformation initiale de 1,0 × 10-3 s-1, ne montrent aucun changement significatif en terme d'élongation maximale et pour la déformation des échantillons mis en solution et recuits à 473 K. Le vieillissement à 523 K conduit à une augmentation de la ductilité quel que soit le nombre de tours et l'allongement maximal de 230% a été enregistré après 20 tours. Une analyse semi-quantitative des microtextures, obtenues à l'aide de l'EBSD et fondée sur le calcul de la fonction de distribution des orientations (FDO) révèle la présence des composantes de texture de torsion mentionnées dans la littérature pour les matériaux c.f.c. En particulier, la composante C {001} <110> est majoritaire. Par ailleurs, aucun changement significatif de l'acuité de la texture a été observé lorsque le nombre de tours augmente.

Mots clé : *les alliages AlMgSi, deformation plastique sévère, HPT, Microstructure, EBSD, Texture , Essais de traction, Dureté*

Abstract

The present work aims to reveal the microstructural evolution and mechanical behavior of a commercial Al-0.6% Mg-0.4% Si alloys subjected to severe plastic deformation. The plastic deformation is applied using high pressure torsion (HPT) which was conducted under a pressure of 6.0 GPa. Before HPT, the discs are solution-treated at 813 K for 2h and then shortly (5min) aged at 473 K and 523 K. The discs in solid-treated and aged conditions are strained to a maximum of 20 turns. Microstructural and mechanical properties evolution of the discs in these three conditions was reported using electron back-scattered diffraction (EBSD), microhardness and microtensile tests. A significant grain refinement was obtained after only 1 turn to achieve an average grain size of about 250 nm after 20 complete revolutions with an increase of hardness up to a saturation value at equivalent strains above ~100. The fraction of high-angle grain boundaries increases with increasing strain. A correlation between the evolution of hardness and grain size seems to obey the conventional Hall-Petch relation for relatively large grain sizes but deviates significantly below 500 nm. This deviation was explained and is consistent with an earlier suggestion that a breakdown may occur if there is an easy movement of the extrinsic dislocations in the non-equilibrium grain boundaries introduced by HPT processing. Tensile test results, conducted at the temperature of 813 K with an initial strain rate of 1.0×10^{-3} s^{-1}, show no significant change in the maximum elongation and during deformation for the solution-treated samples and annealed at 473 K. Aging at 523 K leads to an increase of ductility for all the samples where the maximum elongation of 230% was recorded after 20 turns. Qualitatively microtextures results, obtained using EBSD, based on orientation distribution function (ODF) calculation reveals the presence of the torsion texture components often reported in the literature for f.c.c. materials. In particular, the C {001}<110> component was found to be dominant. Furthermore, no significant change in the texture sharpness was observed by increasing the strain.

Keywords: *AlMgSi alloy, Severe plastic deformation, HPT, Microstructure, EBSD, Texture , tensile test, Hardness*

ملخص

يهدف هذا العمل لدراسة تطور البنية المجهرية و الخواص الميكانيكية لسبيكة Al-0.6% Mg-0.4% Si تجارية من الألمنيوم خضعت لتشوه لدن حاد باستخدام جهاز فتل تحت ضغط عال (HPT) قيمة هذا الضغط 6.0 GPa. عولجت الأقراص معالجة حرارية في درجة حرارة 813 K خلال زمن قدره ساعتين ثم خضعت لتعتيق لمدة قصيرة (5 دقائق) في درجات الحرارة 473 K و 523 K ثم خضعت لعملية التشوه , في الشروط الثلاثة من المعالجة, حتى 20 دورة . تمت دراسة البنية الميكروسكوبية, الميكرونسيج و الخواص الميكانيكية باستخدام جهاز انعراج الإلكترونات المرتدة (EBSD) , الميكروصلادة و الشد الميكانيكي. بينت النتائج المتحصل عليها ان طول الحبوب قد خفض بشكل واضح الى قيمة تعادل 250 nm بعد 20 دورة كاملة مما ادى الى ارتفاع في الصلادة و التي تؤول الى تشبع عند بلوغ التشوهات المكافئة حوالي القيمة 100 وان نسبة حدود الحبوب التي تملك زوايا كبيرة تزداد بازدياد التشوه. العلاقة بين الصلادة و طول الحبوب تخضع لقانون Hall-Petch عند قيم كبيرة نسبيا لأطوال الحبوب و لكن تنحرف عندما تبلغ هاته الحبوب طولا أقل من 500 nm. فسر هذا الانحراف على ان هذا القانون لا يصبح صالحا بسبب حركة التزحزحات الخارجية الى حدود الحبوب في حالة عدم التوازن الترموديناميكي. نتائج اختبار الشد الميكانيكي, والذي اجري عند درجة حرارة 813 K و سرعة تشوه ابتدائية $1 \times 10^{-3}\ s^{-1}$ ، 0. لا تظهر اي زيادة ملحوظة في الليونة للأقراص التي عولجت علاج التجانس الحراري و تلك التي خضعت لتعتيق عند درجة حرارة 473 K .بينما التعتيق عند 523 K ادى الى زيادة في الليونة حيث بلغت الاستطالة القصوى القيمة 230% بعد 20 دورة. ان التحليل الشبه كمي للمكرونسيج, التي حصل عليها بواسطة استنادا على حساب الدالة لتوزيع المتجهات (ODF) بينت وجود مكونات نسيج الفتل المذكورة في الدراسات السابقة للمواد f.c.c وعلى وجه الخصوص المركب C {001}<110> هو الغالب و من ناحية اخرى لم يلاحظ تغير ملحوظ في حدة النسيج مع زيادة دورات الفتل.

كلمات الدليلية : سبيكة *AlMgSi*, تشوه لدن حاد, *HPT* , البنية المجهرية, النسيج , الشد الميكانيكي, , الميكروصلادة.

List of figures

List of tables

Table of contents

Chapter 2: Material and Experimental Procedures

Chapter 3 : Microstructure and Microtexture Evolution during HPT

Chapter 4 : Mechanical Properties after HPT

General Introduction

Nanoscale science and technology is experiencing a rapid development and nano-materials have made a profound impact on every field of materials research. Scientists believe that the nanoscale science and technology will bring revolutions in human history due to the unique properties of nanomaterials. Two basic and complementary approaches have been developed for the synthesis of nanomaterials which are generally termed the ‘‘bottom-up” and ‘‘top-down” procedures.

In the ‘‘bottom-up” procedure, the bulk solids are fabricated through the assembly of individual atoms or nanoparticulate solids. Examples of this approach include inert gas condensation, electrodeposition and ball milling with subsequent consolidation. These approaches have the capability of producing materials with exceptionally small grain sizes. However, the finished products have some contamination introduced during processing (for example, from the ball milling) and there is invariably at least a low level of residual porosity. The ‘‘top-down” approach avoids the introduction of either contaminants or porosity by taking a bulk solid with a relatively coarse grain size and then processing it to refine the grain size to at least the submicrometer level using severe plastic deformation (SPD) method. This method has emerged, during the last two decades, as a widely known procedure for the grain refinement of metals and alloys into sub-micrometer or even nanometer range. Material processed by SPD has shown superior mechanical properties such as high strength, excellent fatigue life, high toughness and low temperature superplasticity. This finds applications in aerospace, automobile, transportation, food and chemical processing, electronics, and conventional defense industries. Among the SPD techniques currently available, equal-channel angular pressing (ECAP) and high-pressure torsion (HPT) are those used most frequently. However, whereas ECAP is able of producing relatively large bulk samples, HPT is used for small samples, generally in the form of disks, and it is ideal for processing hard materials because of the presence of a large hydrostatic pressure. An important feature is that the sample dimensions

remain unchanged during deformation which can lead to imposing a meaningful accumulation of very high strain into a bulk specimen. Indeed, a very significant grain refinement is achieved which cannot be obtained by traditional methods. Both techniques have been used extensively to process a range of different metallic materials leading to exceptional structural refinement and superior properties including high strength at ambient temperature and superplastic capabilities at elevated temperatures. At the present time, HPT is currently the most promising one since it can result in a much refined microstructure with a higher fraction of high angle grain boundaries. Very extensive work on this area has demonstrated that HPT is an effective tool for producing aluminum-based alloys in the subgrain or nanomaterial range. As the main objective of the present work is to establish a qualitative relationship between the microstructure and microtexture evolution in HPT processing of a commercial Al alloy and their effect on mechanical properties, emphasis is also placed on the effect of the aging treatment on the microstructure and the mechanical behavior.

The sequence of the thesis is as follows. A general review on the SPD methods is presented in the first chapter in concentrating on HPT. By this method, a commercial Al-Mg-Si alloy was deformed to produce a bulk ultrafine-grained structure. Experimental procedures undertaken to carry out HPT processing and materials characterization have been given in chapter 2. In Chapter 3 the results of the evolution of microstructure and microtexture during the deformation process by the intense HPT up to 20 turns is presented using EBSD analysis. This technique allows us to obtain crystallographic orientation maps, the average grain size and the distribution of grain boundary misorientations. The texture evolution was determined using orientation distribution function (ODF) analysis calculated from the EBSD measurements. In chapter 4, the strength of our sample at room temperature is estimated in terms of the relation between Vickers microhardness and grain size. Furthermore, the microtensile tests are used to study the mechanical properties evolution at high temperature. Finally, a summary of results and an outlook for further work within the scope of this thesis are presented in the conclusion.

Chapter 1

Literature Review

1. Introduction

During the last two decade severe plastic deformation (SPD) has emerged as a widely known procedure for the grain refinement of metals and alloys into sub-micrometer or even nanometer range. Synthesis of ultrafine-grained (UFG) materials by SPD refers to various experimental procedures of metal forming that may be used to impose very high strains on materials leading to exceptional grain refinement. For production of bulk UFG materials with equiaxed microstructure and high angle grain boundary misorientation, accumulative roll bonding (ARB), equal channel angular pressing (ECAP) and high pressure torsion (HPT) are the three well known SPD methods. In this chapter a short review is given on these techniques in particular HPT which is the deformation process used in our work.

2 Microstructural fragmentation by plastic deformation

Plastic deformation is known to be governed by the formation, movement and storage of dislocations. With increasing strain, the rising density of dislocations is not randomly stored in the microstructures but they are distributed into fairly regular microstructures, with characteristics that depend on process and material parameters. During the first stage of deformation, the grains are divided, change shape and elongate in the solicitation direction.

A substructure of dislocations appears in grains, depending on their crystallographic orientation *[Hughes and Hansen, 1991].* The subdivision of grains results a cellular configuration (cell-blocks) consisting of "walls" having high dislocation density and surrounding the volumes with low dislocation density. With increasing the rate strain, the cell walls are refined to form sub-boundaries (Fig. 1.1). This transformation is accompanied by a decrease in cell size *[Hughes, 2000]* and by a gradual increase in their disorientation (1° to about 5°). The cells blocks-boundaries are known as Dense Dislocation Walls (DDW) *[Hansen, 1992].*

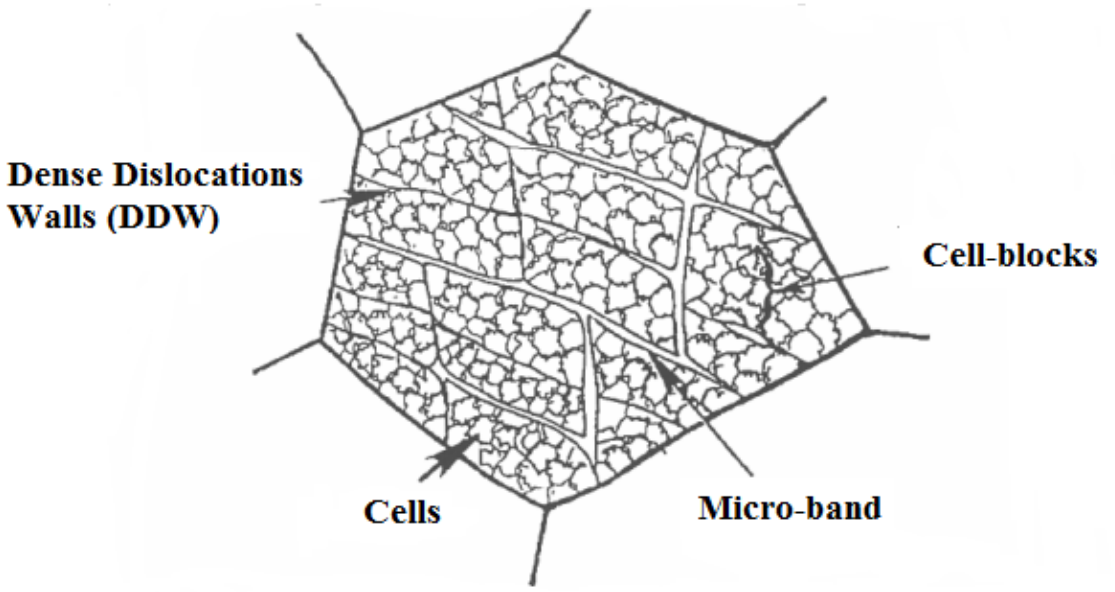

Fig. 1.1: Cell blocks and dense dislocation walls ***[Bay et al., 1992].***

For large strains, other forms of heterogeneities appear:

- Micro-bands formed by dislocation cells with smaller size than the average value of dislocations within cells of the same material.
- Shear bands, typically at 30 or 40° to the solicitation direction, in the form of long bands with a thickness 0.1 to 2µm and 10 to 100 µm in length *[Doherty et al., 1997].* The strain localization in these bands is more important when the temperature and stacking fault energy are low.
- The transition bands separate the adjacent highly disoriented zones of the same grain. They are often parallel to the deformation direction.

The plastic deformation also creates a significant amount of defects such as vacancies and interstitials. A large part of the defects are eliminated either during the deformation (dynamic recovery if T ≥ 0.2 T m), or during subsequent annealing at low temperatures.

3. SPD processes

3.1 Accumulative Roll Bonding (ARB)

In this process (Fig.1.2), thin sheets of metal/alloy are taken and stacked together for roll bonding. The surfaces to be joined are roughened and cleaned; the two parts are stacked and roll bonded with 50% reduction in thickness ***[Saito et al., 1999].***

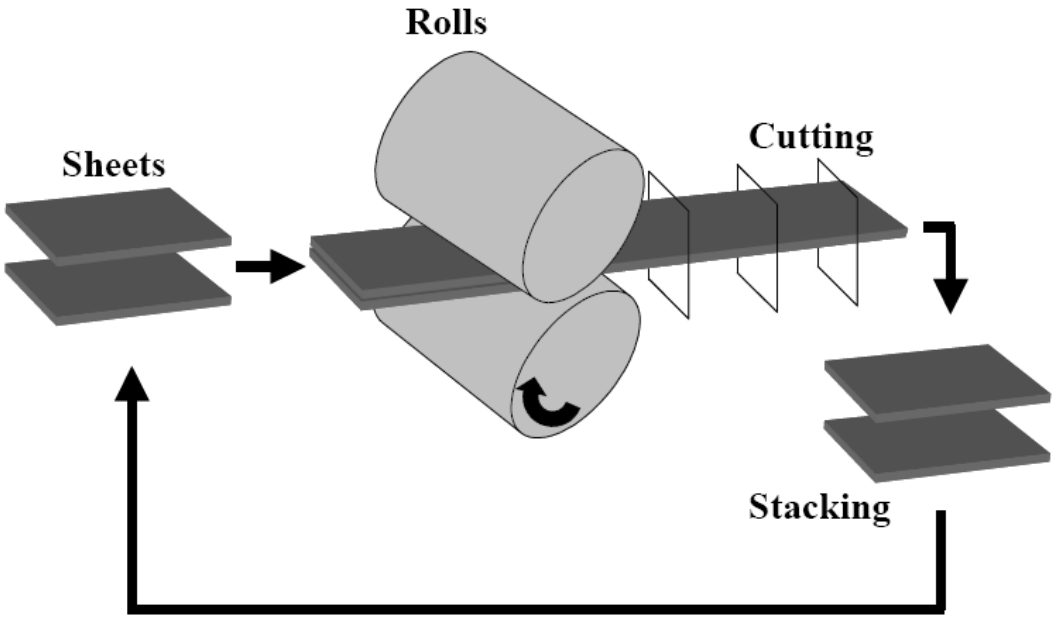

Fig.1.2: *Schematic diagram showing ARB process* ***[Saito et al., 1999].***

The bonded sheet is cut into two halves and again stacked after proper surface cleaning and rolled. The process may be repeated several times. The assumption of the von Mises equivalent plastic strain is ***[Krallics and Lenard, 2004]:***

$$\varepsilon = \frac{2}{\sqrt{3}} \ln\left(\frac{t_0}{t_{final}}\right)^n \qquad \textbf{(1.1)}$$

where t_0 is the initial thickness of strips and n the number of cycles.

3.2 Equal Channel Angular Pressing (ECAP)

Equal-channel angular pressing (ECAP) is the most studied SPD processing technique *[Valiev and Langdon, 2006]*. It is an interesting and demandable method for modifying microstructure in producing ultrafine grained (UFG) materials. A schematic diagram of ECAP is shown in Fig.1.3. In this process a rod/square shaped billet is pressed through a die constrained within an equal channel cross section, which is bent at an abrupt angle.

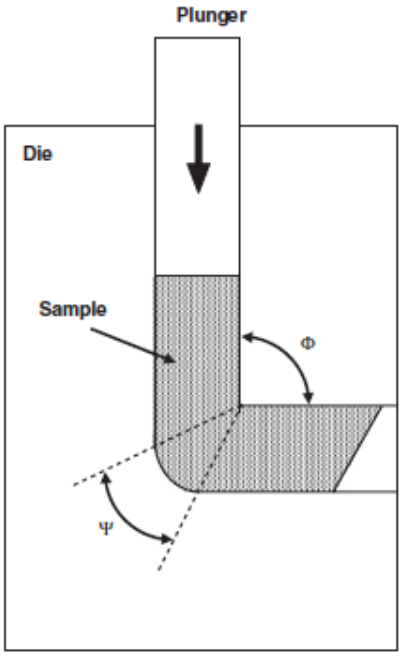

Fig.1.3: Schematic illustration of ECAP [Valiev and Langdon, 2006].

A shear strain is introduced when the billet passes through the point of intersection of the two parts of the channel. Since the cross-sectional dimensions of the billet remain unchanged, the pressings may be repeated to attain exceptionally high strains.

The von Mises equivalent strain ε, introduced in ECAP, is determined by a relationship given in the equation 1.2, incorporating the angle (ϕ) between the two parts of the channel and the angle (ψ) representing the outer arc of curvature, where the two parts of the channel intersect *[Iwahashi et al., 1996; Meyers et al., 2005]*.

$$\varepsilon = \frac{N}{\sqrt{3}}\left(2\cot\left(\frac{\phi}{2}+\frac{\psi}{2}\right)+\Psi\operatorname{cosec}\left(\frac{\phi}{2}+\frac{\psi}{2}\right)\right) \qquad (1.2)$$

where N is the pass number.

3.2.1 Processing routes in ECAP

There are four basic processing routes in ECAP and these routes introduce different shear routes during the pressing operation so that they lead to significant differences in the microstructures produced by ECAP ***[Nemoto et al., 1998; Horita et al., 2000; Furukawa et al., 2003].***

The four different processing routes are summarized schematically in Fig.1.4. This shows that the sample is pressed without rotation (route A), the sample is rotated by 90° in alternate directions between consecutive passes (route B_A), the sample is rotated by 90° in the same sense (either clockwise or counterclockwise) between each pass (route B_C) and the sample is rotated by 180° between passes (route C).

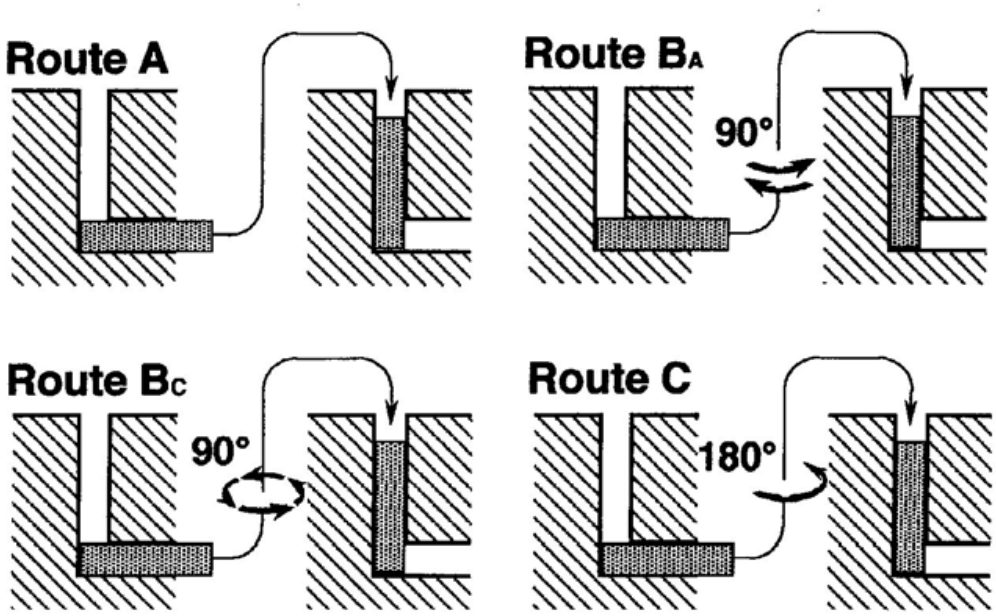

Fig. 1.4: *Processing routes in ECAP.*

3.3 High pressure torsion (HPT)

The scientific origin of processing by HPT may be traced to a classic paper, written by Bridgman and appearing in the Journal of Applied Physics in 1943, entitled ''On Torsion Combined with Compression". In this early report, Bridgman succinctly set out the basic tenets of this type of testing by stating ***[Bridgman, 1943]:***

''If a bar is twisted while a longitudinal compressive load is simultaneously applied, it is possible to twist the bar through much greater angles without fracture than is possible without the compressive load. At the same time the magnitude of the torque which the bar can support without fracture is increased."

The principles of HPT processing are depicted schematically in Fig. 1.5. The sample, in the form of a small disk, is located between two anvils where it is subjected to a compressive applied pressure, P, of several GPa. The disc is subjected to a torsional strain which is imposed through rotation of the lower anvil either at room temperature or at an elevated temperature.

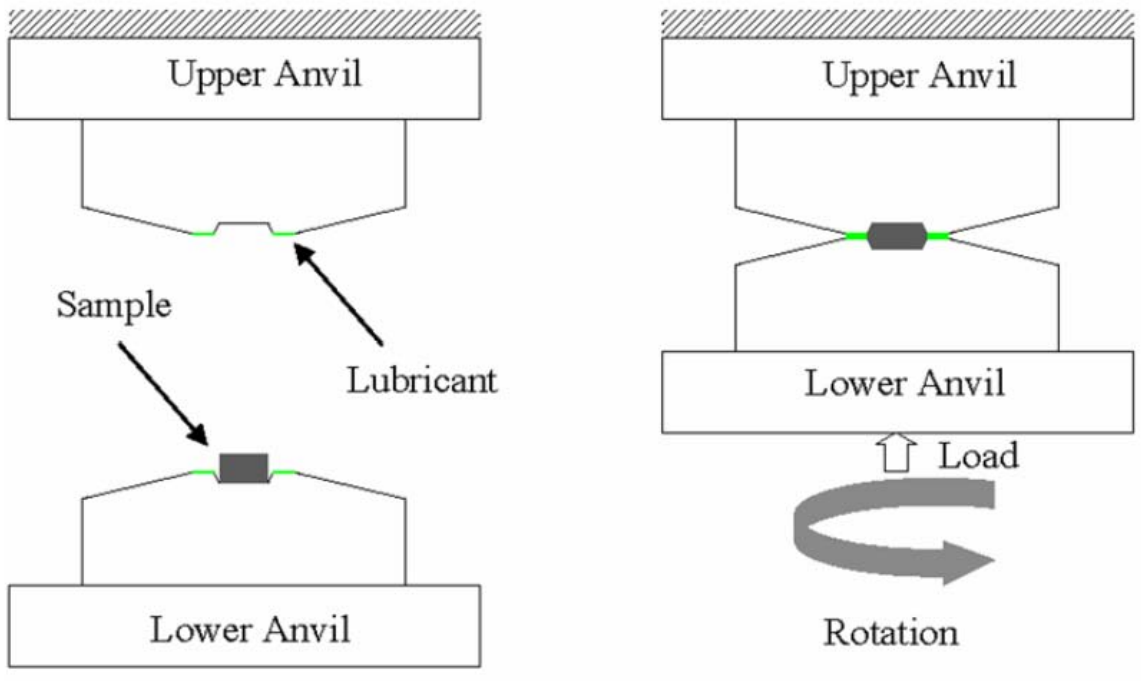

Fig.1.5: Schematic illustration of HPT [Zhilyaev and Langdon, 2008].

The von Mises equivalent strain ε_{eq} is given by the following relationship *[Valiev et al., 1996; Wetscher et al., 2004]:*

$$\varepsilon_{eq} = \frac{2\pi Nr}{h\sqrt{3}} \qquad (1.3)$$

Where N is the number of revolutions, r and h represent the radius and thickness of the disk respectively.

3.4 Comparison between ECAP and HPT

Among the SPD techniques, ECAP and HPT have received a much attention from researchers in this field and two reviews on these processes were recently published *[Valiev and Langdon, 2006; Zhilyaev and Langdon, 2008].* These techniques have been used for a

wide range of materials: pure metals, alloys, composites and ceramics. However, the HPT process has some advantages over the ECAP. Indeed, it can lead to a more pronounced refinement of the microstructure and a higher fraction of high angle grain boundaries *[Zhilyaev et al., 2002; 2005]*. Several studies have also shown that it is possible to have a further refinement of the grain through a combined use of both techniques. The material obtained after ECAE is cut into discs which are then subjected to deformation by HPT. Since the saturation grain size is smaller in HPT than in ECAP, there is the possibility of introducing additional grain refinement by processing using ECAP and then cutting disks and further processing by HPT. This type of approach was confirmed in various Al alloys *[Horita et al., 1996; Mishra et al., 2001; Dobatkin et al., 2002].*

4. State of the art of HPT

4.1 The principles of unconstrained and constrained HPT

In practice there are two distinct types of processing as illustrated schematically in Fig.1.6: these types are termed unconstrained and constrained HPT, respectively *[Zhilyaev et al., 2007]*. In unconstrained HPT, the specimen is placed on the lower anvil and it is then subjected to an applied pressure and torsional straining as illustrated in Fig. 1.6(a). Under these conditions, the material is free to flow outwards under the applied pressure and only a minor back-pressure is introduced into the system due to the frictional forces acting between the sample and the anvil. An example of the use of unconstrained HPT is given by a report of experiments conducted earlier on pure Ni *[Zhilyaev et al., 2003].* In constrained HPT, as shown in Fig. 1.6(b), the sample is machined so that it fits into a cavity in the lower anvil and the load is applied such that there is no outward flow of material during the torsional straining. This means in practice that true constrained HPT is conducted in the presence of an effective back-pressure. However, it is generally difficult to achieve an idealized constrained condition and experiments are often conducted under a quasi-constrained condition as shown in Fig. 1.6(c) where there is at least some limited outward flow between the upper and lower anvils.

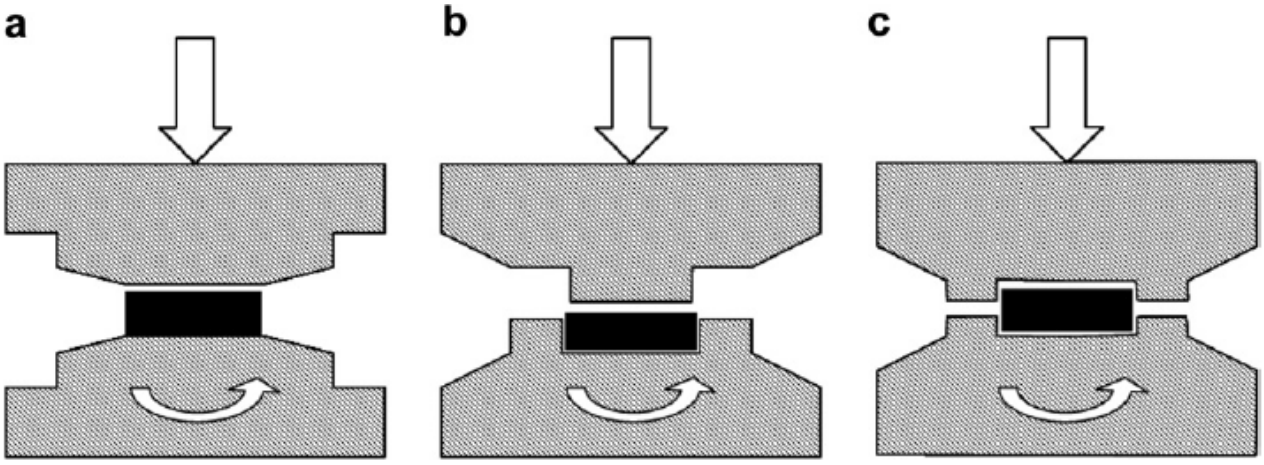

Fig. 1.6: Schematic illustration of HPT for (a) unconstrained and (b, c) constrained conditions ***[Zhilyaev et al., 2007].***

An example of the use of quasi-constrained HPT is given by experiments on an austenitic steel where it was noted specifically that, upon application of the load, there was some limited outward flow of material between the upper and lower anvils ***[Vorhauer and Pippan, 2004].***

4.2 Variation in homogeneity across an HPT disk

An important limitation in HPT is that the imposed strain varies across the sample and, in principle at least, the strain is reduced to zero at the disk center. As a consequence of this variation, it is reasonable to anticipate that the microstructures produced by HPT will be extremely inhomogeneous. Equation (1.3) shows that the imposed deformation directly depends on the position of the point considered in the disk. Indeed, it is maximal at the periphery and no at the center. However, numerous studies have shown that increasing the deformation tends to homogenize the distribution according to the diameter of the disk ***[Zhilyaev et al., 2003; Vorhauer and Pippan, 2004; Sakai et al., 2005a; Xu et al. 2007; 2008a; Xu and Langdon, 2009].*** This contradiction was recently explained using "strain gradient" plasticity model (strain gradient plasticity modeling) ***[Estrin et al., 2008].*** In this approach, the material is in the form of two distinct phases, one corresponds to the cell walls and the other to the dislocations within the cells (or grains). In this model, the change in density of dislocations, ρ_c, inside the cells as a function of time t, is given by the following equation:

$$\frac{d\rho_c}{dt} = A\frac{\dot{\varepsilon}_p\sqrt{\rho_w}}{b\sqrt{3}} - B\frac{6\dot{\varepsilon}_p}{bd(1-f)^{1/3}} - C\left(\frac{\dot{\varepsilon}_p}{\dot{\varepsilon}_0}\right)^{-1/n_{cs}}\dot{\varepsilon}_p\rho_c \qquad (1.4)$$

where A, B and C are constants, $\dot{\varepsilon}_p$ is the von Mises equivalent plastic strain rate, ρ_w is the dislocation density in the cell walls, d is the average dislocation cell size, f is the volume fraction of cell walls, $\dot{\varepsilon}_0$ is a constant having the same dimensions as strain rate and n_{cs} is the recovery exponent for cross-slip which is generally taken as a linear function of the stacking fault energy.

Equation 1.4 is made up of several terms of which the first term on the right of the equality denotes the increase in the dislocation density in the cell walls and the cell interiors due to the activation of Frank–Read sources in the walls; the second term denotes the decrease in the dislocation density in the cell interiors and the third term corresponds to the effect of dynamic recovery and the annihilation of dislocations by cross-slip at large strains. Considering the last term in Equation 1.4, it is immediately apparent that a material such as high purity Al with high stacking fault energy will incorporate a significant influence on the rate and magnitude of the recovery process. However, extensive microstuctural observations will be needed to provide a direct confirmation of this type of model. Using this approach, Fig. 1.7, shows the distribution of accumulated plastic strain along the specimen radius for different numbers of turns in HPT. It can be seen from Fig. 1.7(a) that plastic strain accumulates initially at a very high rate at the edge of the specimen while having a relatively low value in a broad area around the center. On further straining, this difference is gradually reduced as the rate of accumulation of strain in the center exceeds that at the edge, thereby leading to a reasonably uniform strain distribution after 5 turns in Fig. 1.7(b). This increasing homogeneity in the strain distribution is a direct consequence of the evolution of the second-order strain gradient.

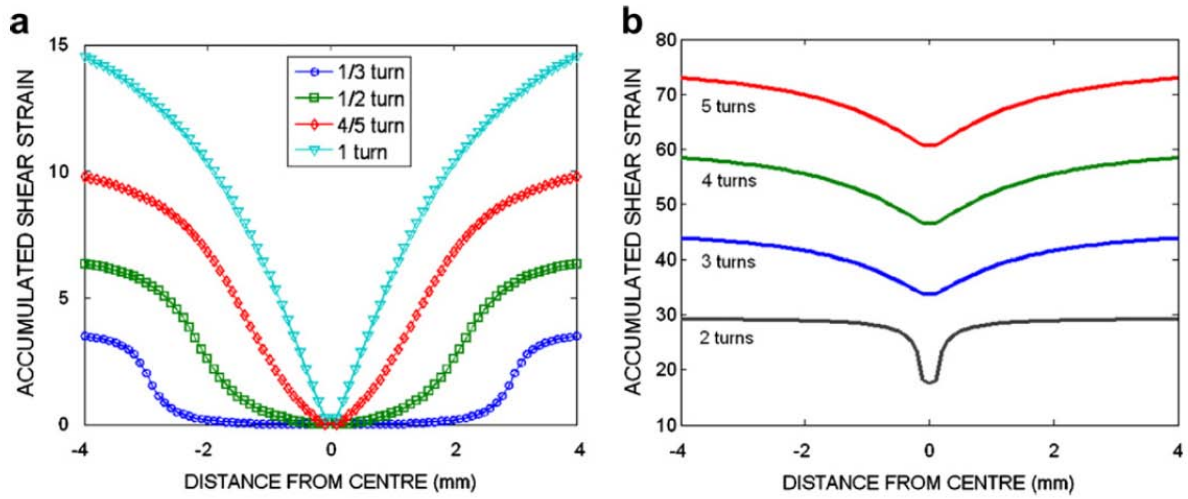

Fig. 1.7: Accumulated equivalent strain versus distance from the specimen center in the first-order strain gradient model ***[Estrin et al., 2008].***

4.3 Influence of the rotation number on the microstructural evolution

The total imposed strain, as measured by the number of revolutions, is also an important factor in processing by HPT. Representative results are shown in Fig. 1.8 where Ni was subjected to an applied pressure of 6 GPa and then torsionally strained through (a) 1/2, (b) 1, (c) 3 and (d) 7 turns ***[Zhilyaev et al., 2003]***. For the condition where N = 1/2 revolution shown in Fig.1.8a, much of the increase in the value of the microhardness relative to the initial value of ~1.4 GPa is a direct consequence of the compression of the disk occurring on application of the applied pressure. However, inspection of all four disks shows there are again regions of higher microhardness near the periphery, as is especially evident after 1 whole revolution, and these regions move towards the center of the disk so that at N = 7 revolutions the local values of Hv are fairly homogeneous across the disk and the average measured local hardness has increased to >3 GPa.

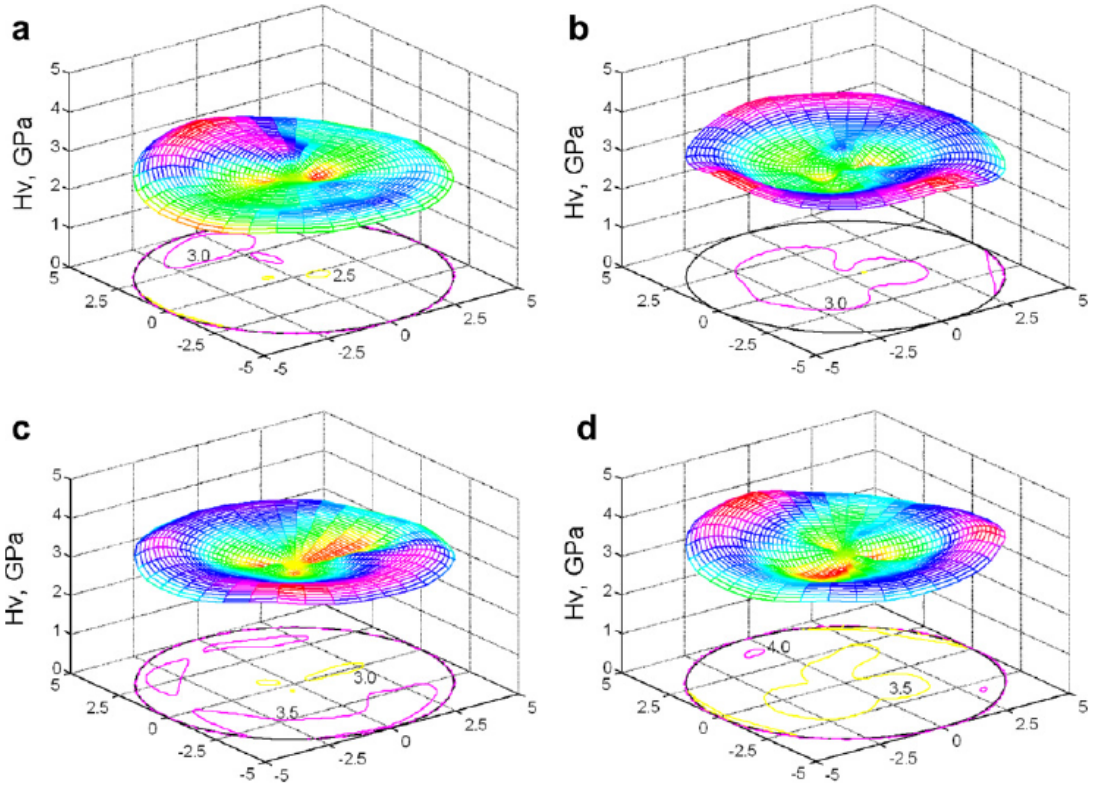

Fig. 1.8: Three-dimensional meshes of microhardness in nickel processed by HPT as a function of the number of turns at a pressure of 6 GPa: (a) N = 1/2 turn, (b) N = 1 turn, (c) N = 3 turns and (d) N = 7 turns ***[Zhilyaev et al., 2003]****.*

4.4 Developing a pictorial representation of the microhardness distribution

Anew approach was developed recently for evaluating microstructural inhomogeneities in samples processed either by ECAP ***[Xu and Langdon, 2003]*** or by HPT ***[Xu et al., 2007].*** In this procedure, the microhardness values are recorded in a rectilinear grid pattern across the sectioned planes of samples and the results are plotted in Fig. 1.9. The form of color-coded contour maps provides an immediate visual representation of the local variations in hardness over the cross-section.

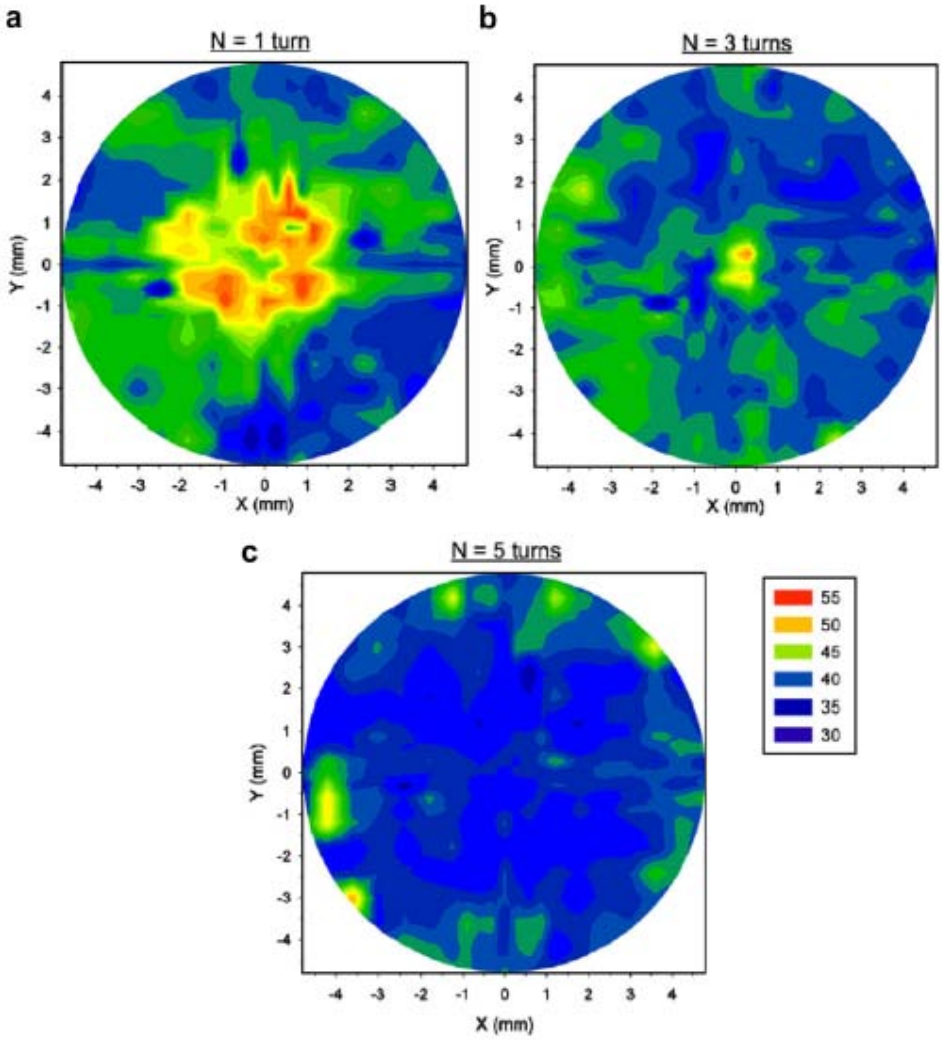

Fig. 1.9: Color-coded contour maps showing the Vickers microhardness across the surface of disks of high purity Al processed by HPT at a pressure of 1.25 GPa for (a) 1, (b) 3 and (c) 5 turns: the significance of the colors is shown by the small inset ***[Xu et al., 2007].***

This technique readily permits a simple and effective monitoring of the local microhardness values on disks processed by HPT under different conditions of pressure and numbers of revolutions. Using this approach, it is possible to evaluate whether the microstructures generated by HPT evolve into truly homogeneous arrays at sufficiently high strains and pressures. The results also provide important new information on the development of homogeneity during HPT processing by demonstrating a direct link between the microstructural evolution in HPT, the applied force and the accumulated strain as represented by the number of revolutions in torsional straining. Furthermore, these inter-relationships are dependent upon the local rate of strain hardening and the rate of dynamic recovery within the material. The microhardness measurements recorded from rectilinear grid patterns, using incremental spacings of 0.3 mm, are plotted as color-coded contour maps

to provide pictorial displays of the distributions of the individual hardness values for each testing condition. Example for high purity aluminum is shown in Fig. 1.9 for a pressure of 1.25 GPa after 1, 3 and 5 turns. In this representation, X and Y denote two arbitrary orthogonal axes which are marked in mm such that the position (0, 0) is at the mid-point of each disk.

4.5 Evolution of the torsion texture

The HPT is a technique not only known for its potential for grain refinement of bulk materials but also associated with the development of specific crystallographic textures that may favor certain properties. Indeed, the texture development in metal torsion of fcc structure can be described by several components of the two {111} <uvw> fibers (α fiber) and {hkl} <110> (β fiber) ***[Montheillet et al., 1984; Tóth et al., 1989]*** typically observed for metals of bcc structure. {hkl} <uvw> represent families of planes and directions respectively parallel to the plane (r, θ) and θ direction. The axes r, θ and z mark the sample are shown schematically in Fig.1.11. The various ideal components observed in the fcc structure materials are collected in Table 2 ***[Montheillet et al. 1984, Tóth et al. 1989; 2004; Zhilyaev et al., 2006a; 2006b].*** The textures are dependent on the crystal structure and were determined for the fcc structure of materials and bcc ***[Li et al., 2005]*** and hcp ***[Beausir et al., 2007].*** Fig. 1.12 shows the various ideal components for fcc materials on {111} pole figure and for bcc materials on {110} pole figure.

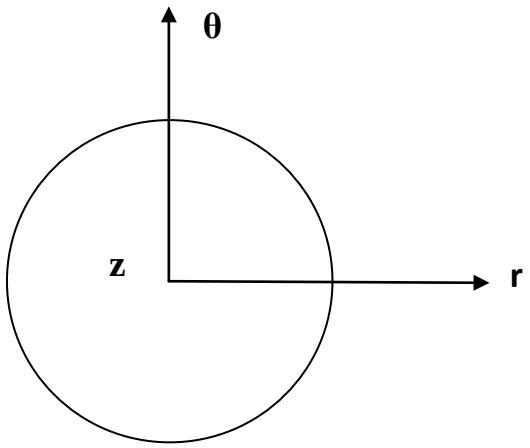

Fig. 1.10: *Representation of directions r, θ and z on a disk.*

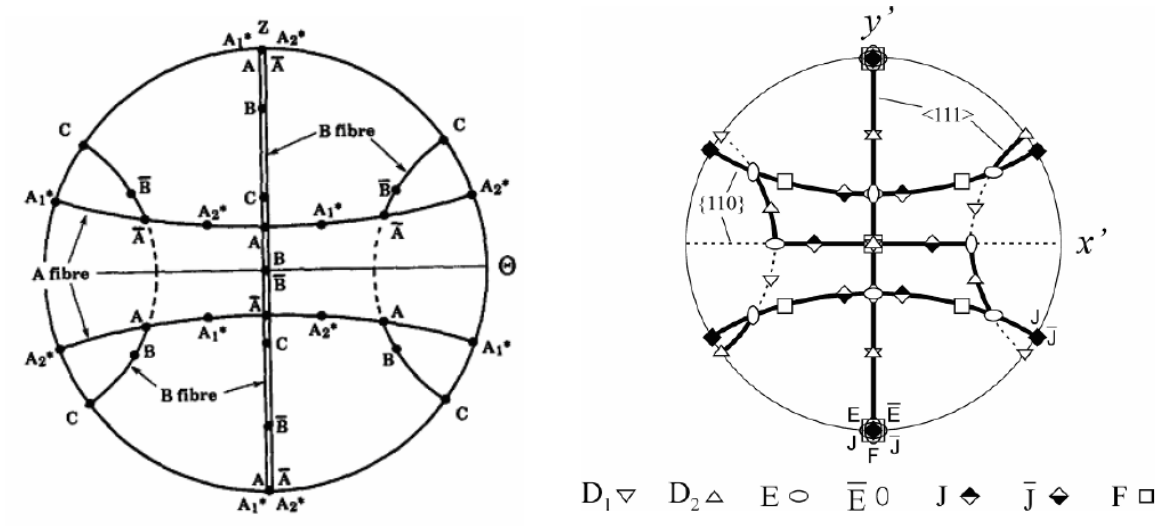

Fig. 1.11: Ideal orientations of torsion textures (a) for fcc materials on an {111} pole figure ***[Tóth et al., 1989]*** *and (b) for bcc materials on a {110} pole figure* ***[Li et al., 2005].***

Table 1.1: *Ideal orientations of torsion textures* ***[Montheillet et al. 1984, Tóth et al. 1989].***

Components	*Shear plane*	*Shear direction*
A	{111}	<110>
A*	{111}	<112>
B	{112}	<110>
C	{001}	<110>

4.6 Mechanical properties after HPT

The most important features of SPD processing is that it leads to an exceptional grain refinement and thereby provides an opportunity to significantly enhance the properties of materials as well as to attain novel and/or unique properties. Among the mechanical tests, tensile testing is certainly the most widely used. It is used to identify key mechanical properties such as elastic modulus, Poisson's ratio, yield strength, the tensile strength, and elongation after fracture. Superplasticity is the ability of some fine-grained polycrystalline materials to undergo extensive plastic deformation caused by a tensile load conditions and specific temperature, without the occurrence of necking before failure. Three parameters influence the superplasticity of metallic alloys: strain rate, grain size and temperature.

Langdon *[Langdon, 2009]* showed that if the material is superplastic elongation reaches a value of at least 400%. Although a pronounced grain refinement is found after HPT, little work concern the effect of HPT on the mechanical properties of materials. This limitation is mainly due to disks that are very thin and the difficulties associated with the preparation of samples Table 1.2 shows the values of elongation to failure after HPT from different studies on a variety of materials *[Kawasaki and Langdon, 2011].* It is apparent from this table that the highest elongation achieved to date is ~1600% when processing an Al–3% Mg–0.2% Sc alloy by HPT using a sample in the form of a small bulk cylinder.

Table 1.2: Maximum elongation to failure to different types of material [Kawasaki and Langdon, 2011].

Material	*Maximum elongation to failure*	*Material shape*
Al–3% Mg–0.2% Sc	~500% ~1600%	Disk Cylinder
Al–4% Cu–0.5% Zr	~800%	Disk
Al-1420	~750%	Disk
Al-1421	~670%	Disk
Al-1570	~1460%	Disk
Al-2024	~570%	Disk
Mg-9%Al	~810%	Disk
Mg-10%Gd	~580%	Disk
Ni_3Al	~560%	Disk
Ti-6%Al-4%V	~570%	Disk

4.7 The processing of aluminum and aluminum-based alloys

Very extensive data are now available for the HPT processing of aluminum-based alloys *[Horita et al., 1996; Senkov et al., 1998; Islamgaliev et al., 2001; Straumal et al., 2004; Dobatkin et al., 2005].* A general conclusion from these reports is that HPT is an effective tool

for producing very substantial grain refinement with the final grain sizes lying typically within the range of ~100–300 nm or even smaller. Examples of exceptionally small grain sizes include the commercial V96Z1 alloy (Al– 7.5% Zn–2.7% Mg–2.3% Cu–0.15% Zr) where the measured grain size was reported as <100 nm ***[Islamgaliev et al., 2001]*** and the Al–3% Mg alloy described earlier where the grain size after HPT was ~90 nm ***[Horita et al., 1996]***. As discussed in later sections, many of these processed alloys exhibit many unique properties including high strength and superior superplastic behavior at elevated temperatures. By contrast, it is interesting to note that the HPT processing of pure aluminum was first documented only very recently when microstructural evolution was investigated in the HPT processing of commercial purity aluminum as a function of the accumulated strain.

4.8 Extension of HPT

The HPT process has undergone a development over last years to extend a large utilization in various fields. For example, as a limitation of this technique is that the sample is small, a configuration able to produce a bulk samples with a diameter larger than 1 cm and a height of 8.57 mm has been developed ***[Sakai et al., 2005b].*** HPT tests on rings have also been proposed. These rings have inner and outer diameters, respectively of 14 and 20 mm and a thickness of 10 mm ***[Harai et al., 2008].*** The HPT also became a process to fabricate pieces from powders, for example from a high-energy ball milling process, such as metal powders of Ni and Co and Fe-1% C, powder $Ti_{60}Cu_{14}Ni_{12}Sn_4Ta_{10}$ metal matrix composites and composite aluminum-fullerene-containing carbon (mixture of C_{60} and C_{70}) ***[Zhilyaev and Langdon, 2008].*** Under the effect of intense plastic deformation, a very good cohesion can be obtained and the final material has generally very little residual porosity, even if the operation takes place at room temperature. It then has a very small grain size and a very high level of hardness.

4.9 Innovation potential for HPT technique

The innovation potential of the nanostructured materials produced by SPD techniques is very high with numerous advanced and functional applications beginning to emerge in the fields of engineering and medicine ***[Valiev et al., 2007].*** The Fig. 1.10 illustrates this potential where it is apparent that the high specific strength of SPD products makes these materials

especially attractive for use under extreme conditions and environments. Examples of the application fields requiring these high strength products extend from the use of titanium and other materials in the aeronautical and defense sectors to the use of specialized steels in arctic environments for oil and gas exploration.

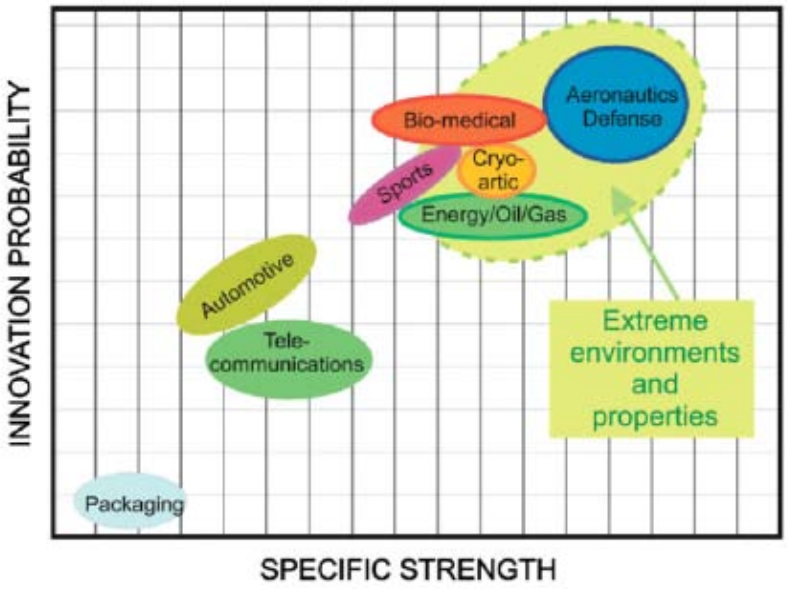

Fig.1.12: The anticipated innovation probability in various sectors versus the specific strength: the highest potential is anticipated in applications and products under extreme environments and/or requiring extreme specific strength ***[Valiev et al., 2007]****.*

From the utilization of parts produced by HPT, it is important to identify specific areas where HPT offers exceptional advantages by comparison with more conventional processing. Based on the information available to date, and the numerous experimental results documented using HPT processing, it is already possible to identify several potential applications for HPT including the following:

- Processing by HPT is ideally suited for the production of the very small parts needed in Micro Electro Mechanical Systems (MEMS) applications.
- The high strength and excellent biocompatibility of several materials makes HPT processing an attractive route for the production of dental and medical implants and for the development of a wide range of mini-components (such as springs, mini-screws, staples) for use in biomedical applications.
- By extending the principles of HPT processing for use with ring or annulus samples, there is a potential for producing washers with excellent mechanical properties.

- The HPT procedure is ideal for use in the consolidation of a wide range of powders and machining chips. This approach can be used for the development of materials for hydrogen storage and other functional applications (for example, with magnetic materials).

5. Conclusion

Based on this review and very recent activity, it is reasonable to anticipate there will be many new developments in this important area over the next decade combined with the emergence of HPT processing as an effective tool for the processing of small parts for use in a range of industrial and medical applications.

References

Bay B., Hansen N., Hughes D.A, Kulhmann-Willsdorf D., Acta Metall. & Mater. 40 (1992) 205

Beausir B., Tóth L.S., Neale K.W. Acta Mater. 55 (2007) 2695-2705.

Bridgman P.W., Appl. Phys. 14 (1943) 273.

Dobatkin S.V., Bastarache E.N., Sakai G., Fujita T., Horita Z., Langdon T.G., Mater. Sci. Eng. A 408 (2005) 141.

Dobatkin S.V., Zhu Y.T., Langdon T.G., Mishra R.S., Semiatin S.L., Saran M.J., Lowe T.C., editors. Ultrafine grained materials II. Warrendale, PA: The Minerals, Metals and Materials Society (2002) 183.

Doherty R.D., Hughes D.A., Humphreys F.J., Mater. Sci. Eng A 238 (1997) 219.

Estrin Y., Molotnikov A., Davies C.H.J., Lapovok R., Mech J., Phys. Solids 56 (2008) 1186

Furukawa M., Horita Z., Langdon T.G., Metals Mater. 9 (2003) 141.

Hansen N., Scripta Metall. & Mater 27 (1992) 1447.

Harai Y., Ito Y., Horita Z., Scripta Mater. 58 (2008) 469.

Horita Z., Furukawa M., Nemoto M., Langdon T. G., Mater. Sci. Tech. 16 (2000) 1239.

Hughes D.A. and Hansen N., Mater. Sci. Tech. 7 (1991) 544.

Horita Z., Smith D.J., Furukawa M., Nemoto M., Valiev R.Z., Langdon T.G., Mater. Res. 11(1996) 1880

Hughes D.A., Proceedings of the Sixteenth Risø International Symposium on Material Science, Edited by N. Hansen, D. Juul Jensen, Y.L. Liu, B. Ralph, Roskilde, Denmark (2000) 63.

Islamgaliev R.K., Yunusova N.F., Sabirov I.N., Sergueeva A.V., Valiev R.Z., Mater. Sci. Eng. A 877(2001) 319–321.

Iwahashi Y., Wang J., Horita Z., Nemoto M., Langdon T.G., Scripta Mater. 35 (1996) 143.

Kawasaki M., Langdona T. G., Mater. Sci. Eng. A 528 (**2011**) 6140–6145.

Krallics G., Lenard J. G., Mater.Proc.Tech. 152 (**2004**) 154.

Langdon T.G., Mater. Sci. 44 (**2009**) 5998.

Li S, Beyerlein I.J., Bourke M.A., Mater. Sci. Eng., A 394 (**2005**) 66-77.

Meyers M.A., Mishra A., Benson D, Prog. Mater. Sci. (**2005**) 443.

Mishra R.S., Valiev R.Z., McFadden S.X., Islamgaliev R.K., Mukherjee A.K., Philos. Mag. A 81 (**2001**) 37.

Montheillet F., Cohen M., Jonas J.J., Acta Metall. 32 (**1984**) 2077.

Nemoto M., Horita Z., Furukawa M., Langdon T.G., Metals Mater. 4 (**1998**) 1181

Sakai G., Horita Z., Langdon T.G., Mater. Sci. Eng. A 393 (**2005a**) 344.

Sakai G., Nakamura K., Horita Z., Langdon T.G., Mater. Sci. Eng. A 406 (**2005b**) 268.

Saito Y., Utsunomiya H., Tsuji N., Sahai T. Acta mater 47 (**1999**) 579-583.

Senkov O.N., Froes F.H., Stolyarov V.V., Valiev R.Z., Liu J., Nanostructure Mater. 10 (**1998**) 691.

Straumal B.B., Baretzky B., Mazilkin A.A., Phillipp F., Kogtenkova O.A., Volkov M.N., Acta. Mater. 52 (**2004**) 4469.

Tóth L.S., Massion R.A., Germain L., Baik S.C., Suwas S., Acta. Mater. 52 (**2004**) 1885.

Tóth L.S., Neal K.W., Jonas J.J., Acta. Metall. 37 (**1989**) 2197.

Valiev R.Z., Ivanisenko Yu.V., Rauch E.F., Baudelet B., Acta. Mater. 44 (**1996**) 4705.

Valiev R. Z.,.Langdon T.G., Prog. Mater. Sci. (**2006**) 881-981.

Valiev R.Z., Zehetbauer M.J., Estrin Y., Höppel H.W., Ivanisenko Y., Hahn H., Adv. Eng. Mater. 9 (**2007**) 527.

Vorhauer A., Pippan R., Scripta Mater. 51 (**2004**) 921.

Wetscher F., Vorhauer A., Stock R., Pippan R., Mater. Sci. Eng. A 809 (**2004**).387–389.

Xu C., Horita Z., Langdon T.G., Acta. Mater. 55(**2007**)203.

Xu C., Horita Z., Langdon T.G., Acta Mater. 56 (**2008a**) 5168.

Xu C., Langdon T.G., Mater. Sci. Eng. A 503 (**2009**) 71.

Xu C., Langdon T.G., Scripta Mater. 48 (**2003**) 1.

Zhilyaev A.P., Kim B.K., Nurislamova G.V., Baró M.D., Szpunar J.A., Langdon T.G., Scripta Mater. 46 (**2002**) 575.

Zhilyaev A.P., Kim B.K., Szpunar J.A., Baró M.D., Langdon T.G., Mater. Sci. Eng. A 391 (**2005**) 377.

Zhilyaev A.P., Langdon T.G., Prog. Mater. Sci., 53 (**2008**) 893-979.

Zhilyaev A.P., McNelley T.R., Langdon T.G., Mater. Sci 42 (**2007**) 1517.

Zhilyaev A.P., Nurislamova G.V., Kim B.K., Baró M.D., Szpunar J.A., Langdon T.G., Acta. Mater. 51 (**2003**) 753.

Zhilyaev A.P., Oh-ishi K., Raab G.I., McNelley T.R., Mater. Sci. Eng. A 441 (2006a) 245.

Zhilyaev A.P., Swisher D.L., Oh-ishi K., Langdon T.G., McNelley T.R., Mater. Sci. Eng. A 429 (2006b) 137.

Chapter 2

Material and Experimental Procedures

1. Introduction

The results obtained in this study are discussed in process light conditions and characteristics tools. Indeed, this chapter is devoted to describe the material and the HPT procedure together with the experimental tools such as EBSD analysis, microhardness and tensile tests. HPT tests are undertaken at the Departments of Aerospace and Mechanical Engineering and Materials Science, University of Southern California. EBSD measurements were undertaken at Paris-Sud University, ICMMO laboratory in France.

2. Selection of material for SPD

The material used in this study was a commercial aluminum alloy provided by ERIS Industry (Batna, Algeria). The chemical composition in wt. % of the alloy is given in the table 2.1. This material is within the 6xxx series of Al alloys (AlMgSi alloys) which are of particular interest to both aerospace and automotive industry because of their attractive combination of properties.

Table 2.1: *Chemical composition of the investigated alloy*

Element	Mg	Si	Fe	Cr	Zn	Cu	Ti	Mn
wt. %	0.59	0.43	0.29	0.032	0.19	0.14	0.019	0.118

The benefits of these alloys include strength, formability, weld ability, corrosion resistance and low cost ***[Troger and Starke, 2000].*** The main characteristic of the 6xxx alloys is the tremendous increase in hardness, due to the precipitation of Mg–Si metastable phase upon annealing at intermediate temperatures. Indeed, it is generally accepted that the sequence of phases is in the following form.

SSS → GP → β″ → β' → β(Mg_2Si) ***[Hirth et al., 2001 ; Ohmori et al. 2002; Chakrabarti et al., 2004]***.

SSS → clusters of Si and Mg → Dissolution of Mg clusters → formation of co-clusters Mg/Si → GP → β″ → β' → β(Mg_2Si) ***[Gomes et al. 1998, Wang et al. 2003]***.

- (SSS): supersaturated solid solution of the α-aluminium matrix
- GP: Guinier Preston zones with spherical shapes and unknown structures
- β″: Needles precipitates elongated along the $<100>_{Al}$ directions with monoclinic structures, different parameter values of crystal lattice have been reported ***[Miao and Langdon, 2000; Esmaeili et al. 2003]***.
- β' : Rods Precipitates elongated along the $<100>_{Al}$ directions having a hexagonal crystal structure (a=0.705 nm et c=0.405 nm) ***[Dimier 2003]***.
- β: Equilibrium phase β(Mg2Si) in the form of small plats elongated on $\{100\}_{Al}$ having a structure fcc type CaF_2 (a =0.636 nm) ***[Cayron et al. 1999]***.

Precipitation can occur at room temperature (natural ageing), but an artificial ageing treatment is normally used in order to achieve a more stabilized material with as high a strength as possible. The maximum strength generally occurs when there is a mixture of coherent and semi-coherent precipitates. Overageing produces stable incoherent particles, giving a lower strengthening effect (e.g. so called Orowan hardening).

3. Sample preparation and procedure for HPT

The as-received material was cut into disks of 10 mm diameter and ~1.5 mm thickness and then ground on SiC papers to final thicknesses of ~0.8 mm in order to remove the strained layer affected by the cutting process. A first batch of disks was solution treated at 813 K for 2

hours and then immediately quenched in cold water. A second batch was solution treated at 813 K for 2 hours and then aged for 5 minutes at two different temperatures, 473 K and 523 K. These temperatures are commonly used to causes β″ to precipitate ***[Marioara, 2000]***. This phase is the most efficient hardening in the 6xxx aluminium alloy system. The disks were processed by HPT at room temperature (296 K) using a quasi-constrained facility in which each anvil contained a central circular depression with a diameter of 10 mm and a depth of 0.25 mm [***Zhiyaev and Langdon, 2008]*** . The applied load was ~47 tons giving an initial applied pressure on each disk of 6.0 GPa. Experiments have shown that this pressure is sufficient to avoid the occurrence of any slippage during the processing operation ***[Edalati et al., 2009].*** The rotation speed of the lower anvil was set at 1 rpm: earlier experiments showed that the rotation speed has very minor effect on the development of strengthening within the HPT samples, at least for rotation speeds between 1/2 and 2 rpm ***[Serre et al., 2011].*** The images are taken for the discs before and after deformation which are shown in the Fig. 2.1. The some limited outward flow of material after deformation is shown in figure 2.1b because of using the experiments which are conducted under a quasi-constrained condition.

(a) ***(b)***

Fig. 2.1: *Disks before (a) and after (b) deformation by HPT.*

For the high temperature processing, the upper and lower anvils were initially heated without the sample in place, the heating was terminated on reaching the desired temperature, the anvils were separated and the HPT disk was placed in the central shallow depression of the lower anvil, the anvils were brought back into place so that the sample experienced the selected imposed pressure. The facility was heated to the required temperature, held at temperature for 3 min and then torsional straining was imposed through rotation of the lower anvil.

4. Experimental methods

4.1 Mechanical properties characterization

4.1.1 Hardness test

After HPT processing, hardness tests were conducted on the polished surfaces of the disks using a Zwick Roell ZHV10 micro-hardness tester equipped with a Vickers indenter. A load of 100 g and a dwell time of 10 s were used for all measurements. The hardness values were recorded along the diameters of each disk at positions separated by ~0.5 mm. At every point, the average microhardness was determined from three separate measurements clustered uniformly around the selected position.

4.1.2 Micro-tensile test specimen

An electro-discharge machining was used to cut the disks into miniature tensile specimens having gauge lengths and widths of 1 mm. Two tensile specimens were cut from off-center positions in each disk as illustrated schematically in Fig. 2.2 with the centers of each gauge length located 2 mm from the center of the disk. These off-center positions were used to avoid any microstructural inhomogeneities that may exist near the centers of the disks: it was shown earlier that this is a good procedure for measuring the mechanical properties of materials processed by HPT ***[Dobatkin et al., 2005].*** All specimens were pulled to failure in tension at the solution treatment temperature of 813 K using an Instron testing machine operating at a constant rate of crosshead displacement and with an initial strain rate of 1.0×10^{-3} s^{-1}.

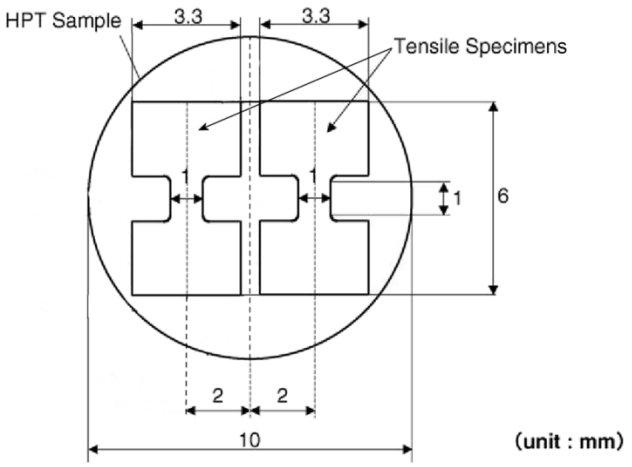

Fig. 2.2: Schematic of tensile test specimen

4.2 Microstructure characterization

4.2.1 SEM/EBSD

Electron backscatter diffraction (EBSD) technique, using Kikuchi patterns produced in scanning electron microscopy (SEM), represents a modern tool to characterize microstructures and textures in crystalline metal and ceramic materials. This technique has a number of advantages over other diffraction methods such as X-ray diffraction because it can provides a local analysis. EBSD allows the study of the following aspects: texture characterization, grain size distribution and grain boundaries nature.

4.2.2 Formation of Kikuchi Patterns

EBSD method is based on the interaction between an incident electrons beam and the sample. The electron back-scattered and their diffraction in contact with the crystal structure form Kikuchi diagrams for determining the crystallographic orientation of the analysis volume. When the electron beam is in contact with the material it is no unidirectional, but, because of collisions with the atoms, it diffuse in all directions. Some of the diffracted electrons verify the law of Bragg which usually written as:

$$2d_{hkl}\sin\theta_B = n\lambda \qquad (2.1)$$

Where n is the diffraction order, λ is the wavelength, d_{hkl} is interplanar spacing of {hkl} plans, θ_B is the angle at which the diffraction takes place. In practice, only the dense planes are visible (small θ_B). The location of the resulting radiation is the surface of an axis cone which coincides with the normal to the plane {hkl} and half apex angle (90° - θ_B). The electron source can be considered between the atomic planes, so that two cones are generated for each family of planes, they are the Kossel cones. Fig. 2.3 illustrated the formation of Kikuchi patterns by EBSD in SEM. The usual values of λ and d_{hkl} conducted via equation 2.1 at θ_B angles of about 0.5°. So, the Kossel cones are almost flat. Their intersections with the observation screen are the conics portions if "flat" they appear to be parallel lines. These are the Kikuchi lines, bounding the Kikuchi bands. All the Kikuchi bands form a Kikuchi pattern. The number of bands depends on the diagram of the solid angle covered by the screen; it must therefore be large enough and close to the analysis zone. Provided that the number of bands is quite large (the respective positions of the bands are analyzed), the diagram completely defines the crystal orientation of the analyzed volume. In practice, a perfectly polished sample, is placed in a scanning electron microscope. The electron beam

must be of sufficient energy (15-30 keV) with a stronger current than standard SEM observation (of the order of 2-3 nA with a standard camera EBSD). The sample is tilted so that the normal to its surface and the electron beam makes an angle of 70° (maximum emission compromise between a back-scattered electron and limitation of the effects of roughness of the sample). The EBSD detector consists of a phosphor screen, on which the back-scattered electrons form the diagram, and a digital camera which takes in real time the diagrams image. These data are then exploited by automatic indexing software which calculates the corresponding crystallographic orientation. A quality index IQ of Kikuchi diagram can also be determined. It describes the average intensity of the diffraction bands from the background noise. This index is very sensitive to local imperfections of the crystal and the grain boundaries. A mapping of this index can accurately visualize the microstructure ***[Germain, 2006].***

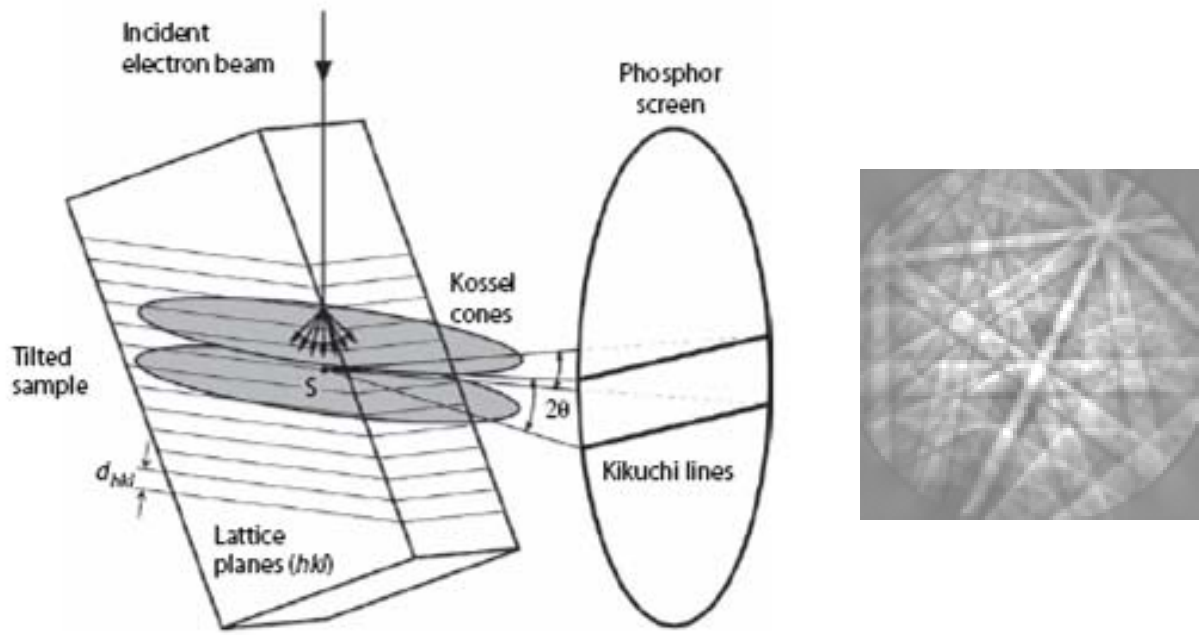

(a) (b)

Fig. 2.3: *(a) Formation of Kikuchi patterns from the crystalline planes {hkl}* ***[Randle and Engler, 2000]*** *and (b) example of Kikuchi pattern.*

4.2.3 Sample preparation for microstructure analysis

Electron back-scatter diffraction was used to characterize the grain structure of the material before and after HPT processing. The information obtained by this analysis included the grain crystallographic orientation maps, the average grain sizes and the distribution of the grain boundaries misorientations. The experimental data were collected using a scanning

electron microscope FEG-SEM SUPRA 55 VP operating at 25 kV with a TSL orientation imaging system, OIM™ software and a cut-off angle of 1° for the minimum boundary misorientation. Samples for EBSD analysis were mechanically ground and then electrolytically polished with an A2 Struers solution. This solution is composed of 910 ml of A2- I solution (65–85% ethanol, 10–15% ethylene glycol monobutyl ether butyl cellosolve and 5–15% water) and 78 ml of A2-II solution (perchloric acid 60%). The scanned area was 1000 µm × 1000 µm with a step size of 5 µm for the unprocessed sample. For the discs processed by HPT, several EBSD analyses were performed taking into account the numbers of applied turns. Thus, the scanned areas were 100 µm × 100 µm with a step size of 0.1 µm for the N = 1 and 5 samples, 50 µm ×50 µm with 0.05 µm for the N = 10 sample and 5 µm × 5 µm with 0.025 µm for the N = 20 sample. These latter maps were important to provide good estimates of the grain size distribution in the ultra-fine microstructures. All deformed microstructures were cleaned with the grain dilation method where the minimum required grain size was equal to two steps. The EBSD analysis used in this study is shown in the Fig. 2.4.

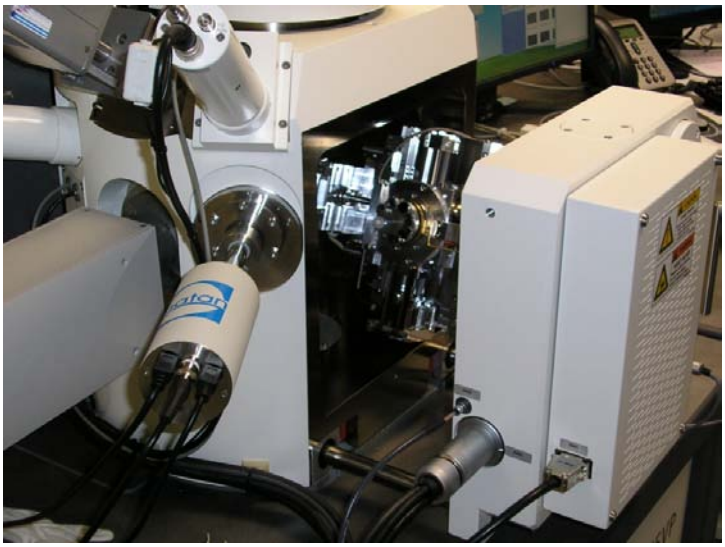

Fig. 2.4: Photo of the MEB chamber showing the 70° tilted sample for EBSD measurement

4.3 Microtextures description and characterization

4.3.1 Microtextures description

4.3.1.1 Direct pole figures

The direct pole figures are used to describe crystallographic textures. Consider a crystal of cubic structure with a given orientation (Fig. 2.5). Normal to the planes of the {001} crystal

"pierced" the sphere of poles of the characteristic points, whose position depends on the orientation of the crystal in the reference sample (RD, TD, ND). We can then use the South Pole project of these points on the equatorial plane (A, B and C). It thus comes to realize the stereographic projection of the three poles {100} is the pole figure {100} crystal considered, that is to say, the stereographic projection of the reference crystal in the reference sample. The direct pole figure of a polycrystalline sample is the stereographic projection on the sample plane of the poles distribution density of the {hkl} planes family in all directions of the sample.

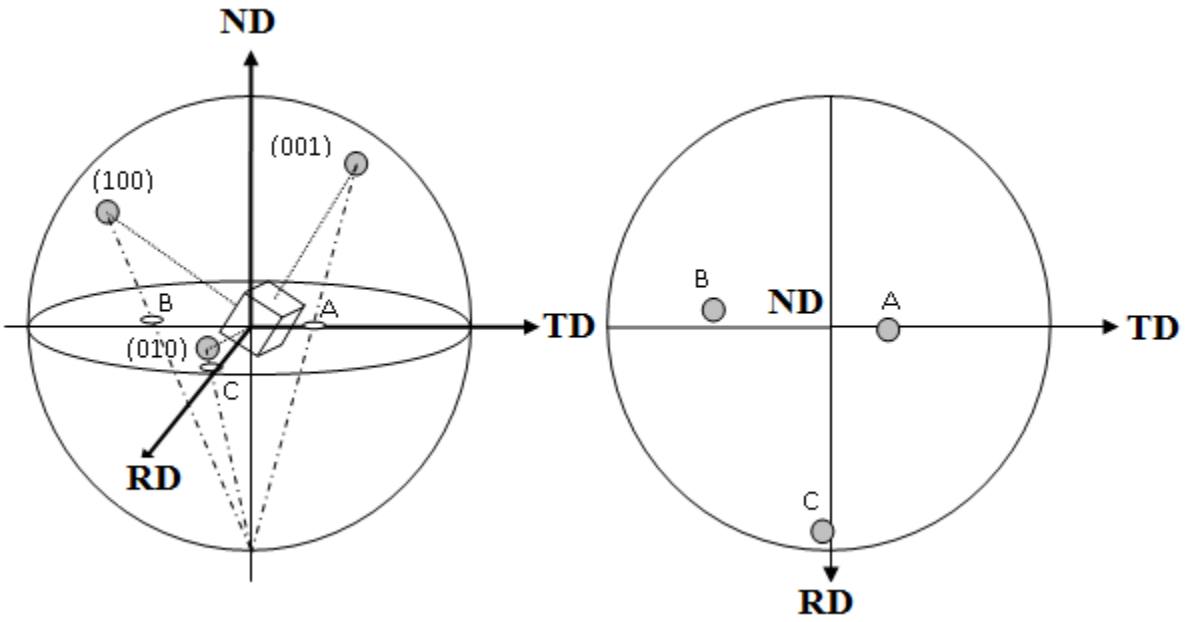

Fig. 2.5: Construction of a pole figure {100}.

4.3.1.2 Inverse pole figures

As it is indicated by its name, the inverse pole figure is a sort of 'opposite' to the pole figure. While the pole figure shows how the specified crystallographic direction of grains are distributed in the sample reference frame, the inverse pole figure shows how the selected direction in the sample reference frame is distributed in the reference frame of the crystal. Since the properties of many important engineering materials are strongly direction-dependent, the inverse pole figure is very useful in predicting and calculating the average properties of polycrystalline material along a chosen direction. They are represented in the

reference crystal. The symmetry of the cubic system gives a possibility of representation in the standard stereographic triangle [001] [011] [111] (Fig. 2.6).

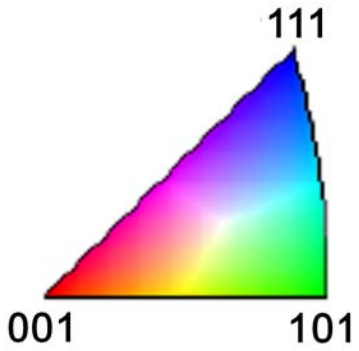

Fig. 2.6: Inverse pole figure for cube materials

4.3.1.3 The Euler Angles

The Euler angles refer to three rotations that, when performed in the correct sequence, transform the specimen coordinate system {E} ≡ (O, RD, TD, ND) onto the crystal coordinate system {C} ≡ (Oxyz). There are several different conventions for expressing the Euler angles. The most commonly used is those formulated by Bunge, as shown in Fig. 2.7 ***[Bunge, 1965].*** The rotations are as follows:

- φ_1 about z axe ;
- ϕ about x axe;
- φ_2 about z axe.

The crystallographic orientation of grains in the sample is denoted g = {φ1, ϕ, φ2} with $0 < \varphi_1 < 2\pi$, $0 < \phi < \pi / 2$, $0 < \varphi_2 < \pi / 2$ for triclinic symmetry texture of a cubic sample. Each point in the three-dimensional Euler space is therefore defined by these three angles.

4.3.1.4 Orientation distribution function (ODF)

The orientation distribution function (ODF) is a function that characterizes the crystalline texture. For a sample having a volume V_0, the ODF f (g) is proportional to the volume fraction ΔV (g) of the grains whose orientation is between g and g + Δg. The ODF is then defined by:

$$\frac{dV(g)}{V_0} = K.f(g).dg \qquad (2.2)$$

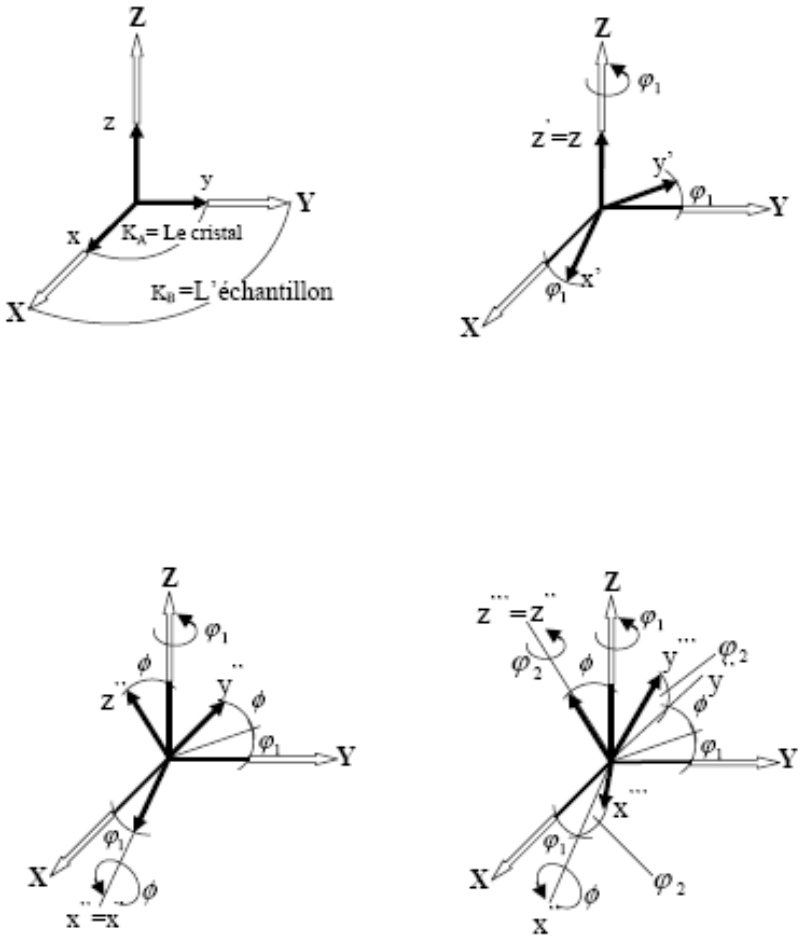

Fig.2.7: *Diagram showing how rotation through the Euler angles φ_1, φ, φ_2* ***[Hansen et al., 1978; Bunge, 1982].***

Different calculation methods are conventionally used to calculate the ODF from pole figures measured by X-ray or neutron diffraction. Among them, the harmonic method is used ***[Bunge, 1982]*** and Roe ***[Roe, 1965].*** This method is also used to calculate an ODF from individual orientations measured by EBSD for example. For using this it is necessary to determined:

$$f(g) = \sum_{l=0}^{L} \sum_{m=-l}^{l} \sum_{n=-l}^{l} C_l^{mn} T_l^{mn}(g) \qquad (2.3)$$

Where f(g) is the ODF function express in Euler space, g is an orientation characterized by the φ_1, ϕ, φ_2 angles, T(g) are the generalized spherical harmonic functions and C are the ODF coefficient which can be calculated from pole figures measured by X-ray or neutron diffraction or from individual orientation measurements. The first problem in the individual orientation measurement case is concentrated on how model each orientation. Bunge *[Bunge, 1982]* suggested modeling each orientation g_i by a Dirac function, the total function f (g) being the sum of N Dirac functions. However, Wagner *[Wagner, 1983]* has showed that this approach leads to negative domains (related to the truncation effects) since the series expansions are calculated for a finite value of L, knowing moreover that by definition the ODF that is the sum total of even odd part and odd part, is always positive or zero:

$$f(g) = \tilde{f}(g) + \tilde{\tilde{f}}(g) \geq 0 \qquad (2.4)$$

Several authors *[Virnich et al., 1978;* Lücke *et al. 1981]* have proposed to use Gaussian functions to express the C_l^{mn} coefficients:

$$C_l^{mn} = \frac{2l+1}{N} \sum_{i=1}^{N} K T_l^{mn}(g) \qquad (2.5)$$

where:

$$K = \frac{exp(-l^2 \phi_0{}^2 / 4) - exp\left[-(l+1)^2 \phi_0^2 / 4\right]}{1 - exp(-\phi_0^2 / 4)} \qquad (2.6)$$

The ϕ_0 parameter is related to half width of the Gaussian by the relation:

$$\phi_0 = b / 2\sqrt{\ln 2} \qquad (2.7)$$

4.3.2 Microtexture characterization

The texture can be characterized by different techniques depending on the scale at which the study is performed. It can be estimated by X-ray or neutron diffraction. These two techniques provide statistical information on the grain orientation which cannot correlate with the microstructure. By contrary, the texture can be obtained using a local approach using EBSD

or TEM. In this study we have specifically used the EBSD technique to estimate the changes in texture depending on the radius of the disk.

5. Conclusion

The different techniques described in this chapter have been successfully used to deform our sample by HPT and then to characterize their microstructural and mechanical properties with number of turns. The obtained results were presented in detail in chapters 3 and 4.

References

Bunge H.J., Texture Analysis in Materials Science, Butterworth, London (**1982**).

Bunge H. J., Z. Metallkd. 56 (**1965**) 872.

Cayron C., Sagalowicz L., Beffort O., Buffat P. A., Phil. Mag. 79 (11) (**1999**) 2833- 2851.

Chakrabarti D. J, Laughlin D. E., Progress Mater. Sci. 49 (**2004**) 389-410.

Dimier F., Ph.D thesis, Superior National School of Mines. Paris (**2003**).

Dobatkin S.V, Bastarache E.N, Sakai G, Fujita T, Horita Z, Langdon T.G., Mater. Sci. Eng. A 408 (**2005**) 141.

Edalati K., Fujioka T., Horita Z., Mater. Sci. Eng. A 497 (**2009**) 168.

Esmaeili S., Wang X., Lloyd D. J., Poole W. J., Met. Mater. Trans. 34(A) (**2003**) 751-762.

Germain L., Ph.D thesis, Paul Verlaine Metz University (**2006**).

Gomes R. M., Sato T., Tezuka H., Kamio A., Mater. Trans JIM. 39(3) (**1998**) 353-364.

Hansen J., Pospiech J., Lücke K., Tables for Textures Analysis of Cubic Metals, Springer Verlag Berlin, Heidelberg New-York, (**1978**).

Hirth S. M., Marshall G. J., Court S. A., Lloyd D. J., Mater. Sci. Eng. A 329-321 (**2001**) 452-456.

Luck K., Pospiech J., Virnich K.H., Jura J., Acta. Metall. 29 (**1981**)167-185.

Marioara C. D., Ph.D Thesis, Norwegian University of Science and Technology (NTNU) (**2000**).

Miao W. F., Laughlin D. E., Met. Mater. Trans. 31(A) (**2000**) 361-371.

Ohmori Y., Doan L. C., Nakai K., Mater. Trans. 43(2) (**2002**) 246-255.

Randle V., Engler O. Introduction to texture analysis. Macrotexture, microtexture and orientation mapping. Gordon and Breach Science Publishers (**2000**).

Roe R. J., Appl. Phys. 36 (**1965**) 4329.

Serre P., Figueiredo R.B., Gao N., Langdon T.G., Mater. Sci. Eng. A 528 (**2011**) 3601.

Troger L.P., Starke E.F., Mater. Sci. Eng. A 277 (**2000**) 102-113.

Virnich H.J., Pospiech J., Flemmer A., Luck K. Proc ICOTOM 5, Aachen, March (**1978**).

Wagner F., Ph.D thesis, Metz University (**1983**).

Wang *X., Poole W. J., Esmaeili S., Lloyd D. J. Embury J. D., Met. Mater. Trans. 34(A) (**2003**) 2913-2918.*

Zhilyaev *A.P., Langdon T.G., Prog. Mater. Sci. 53 (**2008**) 893-979.*

Chapter 3

Microstructure and Microtexture Evolution during HPT

1. Introduction

It is well know that the deformation via HPT is not uniform from the center to the edge disk sample expected to lead to inhomogeneity of the microstructure. As sequence, special attention is devoted to the evolution of microstructure and microhardness under different processing conditions such as number of turns ***[Zhilyaev et al., 2001; 2005; Sakai et al., 2005]***. Indeed, this chapter is initially focused on the microstructures evolution with numbers of turns up to 20 complete revolutions undertaken using EBSD and hardness measurement. Second part of this chapter is devoted to study the microtexture evolution with torsional straining using orientation distribution function (ODF).

2. Microstructures evolution

2.1 Evolution of grain refinement during HPT

The unprocessed material is solid solution and immediately quenched in cold water. The grain structure and the intermetallics are depicted using the EBSD images and SEM

observations, respectively. The typical grain structure in the unprocessed material is shown in Fig. 3.1 together with the color code for the various grain orientations. According to this figure, the microstructure exhibits large equiaxed grain morphology with an average size of about 150 μm.

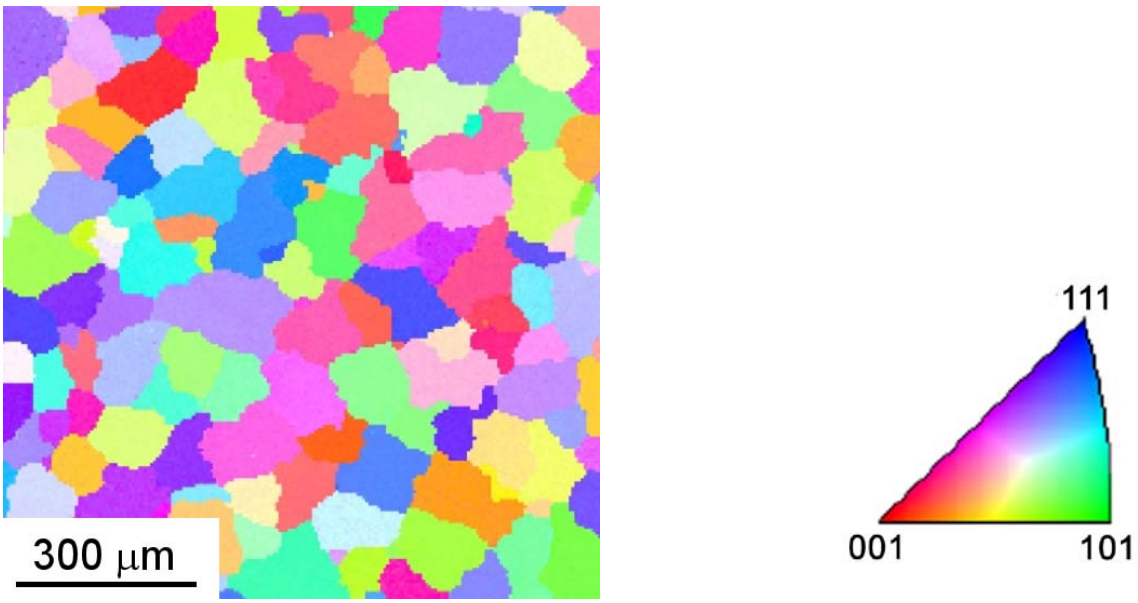

(a) **(b)**

Fig. 3.1: (a) Grain structure of the solution-treated alloy before HPT and (b) the color code used to describe the {hkl} plane of the grains parallel to the disk surface.

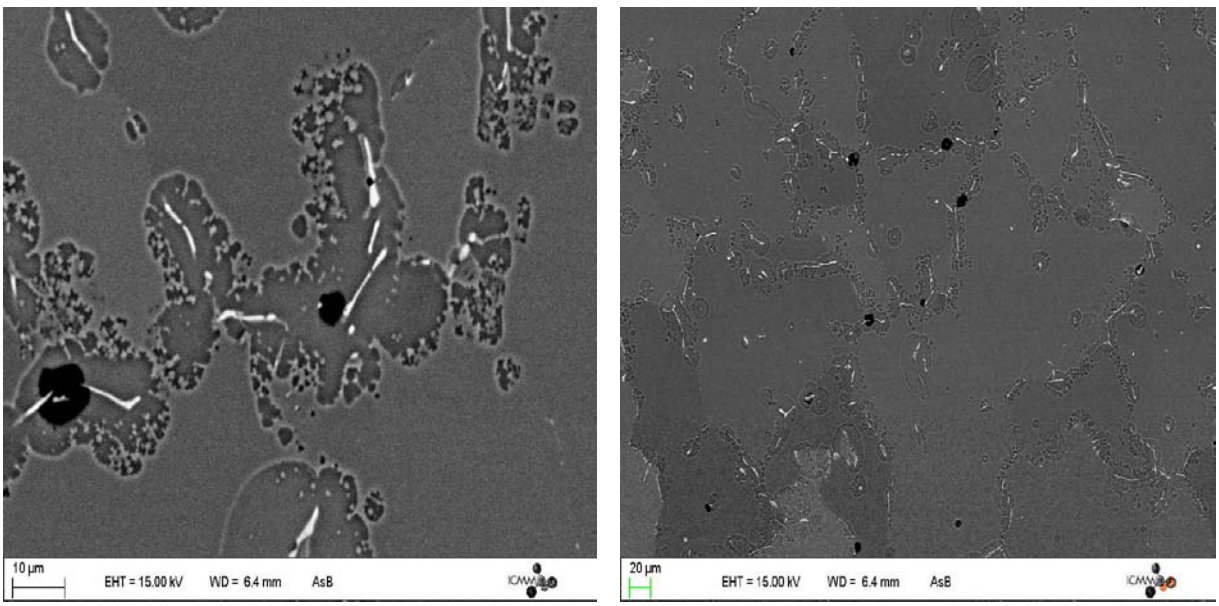

Fig. 3.2: SEM micrograph depicting the dispersoids in solid-treated sample

Fig. 3.2 shows micrographs of the sample used in this study after solid-solution treatment. These images depicted different morphologies of dispersoids aligned along the grain boundaries. Indeed, the three most prevalent intermetallics (dispersoids) in 6xxx Al series alloys are the monoclinic β-AlFeSi phase, the hexagonal α_h-AlFeSi and cubic α_c-Al (FeMn) Si ***[Skinner et al., 1986; Zheng et al., 2000]***.

Fig. 3.3 depicts EBSD maps of microstructure of samples processed through (a) 1 turn, (b) 5 turns, (c) 10 turns and (d) 20 turns of HPT. These structures correspond to the distributions of crystallographic directions parallel to the HPT rotation axis. All of these images were recorded at the mid-radius position of the disks corresponding approximately to the mid-point between the center and the edge. It is apparent from these images that a significant refinement of microstructure is achieved after 1 turns and the average grain size is in the vicinity of about 1 μm. With increasing amounts of deformation imposed by HPT the grain size decreases. Table 3.1 provides a summary of the measured average grain sizes determined by EBSD after the four processing conditions with measurements taken at the center, mid-radius and edge of each disk: the errors on these measurements was estimated at about ±15%. The results show that the grain sizes are smallest at the edge of the disk and largest at the center. In each position the grain size gradually decreases with increasing straining until it attains a saturation size of ~250 nm. This saturation condition is reached at both the edge and the mid-radius after 20 turns but it appears that a small amount of additional straining is needed in order to place the center of the disk into a fully saturated condition. The gradual evolution visible in Fig. 3.3 towards a homogeneous structure is consistent both with earlier results on the Al-6061 alloy ***[Xu et al., 2008a; 2008b; Xu and Langdon, 2009]*** and with experimental data reported for other materials such as high-purity Al ***[Xu et al., 2007]***, an Al–Mg–Sc alloy ***[Sakai et al., 2005]***, high-purity Cu ***[Edalati et al., 2008]***, high-purity Ni ***[Zhilyaev et al., 2003]*** and steel ***[Vorhauer and Pippan, 2004]***.

Close inspection of the grain size evolution in Table 3.1 reveals a very significant structural refinement in the center of the disks after processing to large numbers of turns. Thus, the average grain sizes in the centers of the disks processed by 10 and 20 turns of HPT, equal to 310 and 280 nm, respectively, are significantly smaller than the grain sizes recorded at the mid-radius and edge positions after 1 turn. The demonstration of a saturation grain size in HPT processing is consistent with earlier studies but the physical factors controlling this limitation in refinement are not yet understood ***[Furukawa et al., 1998; Pippan et al., 2010]***.

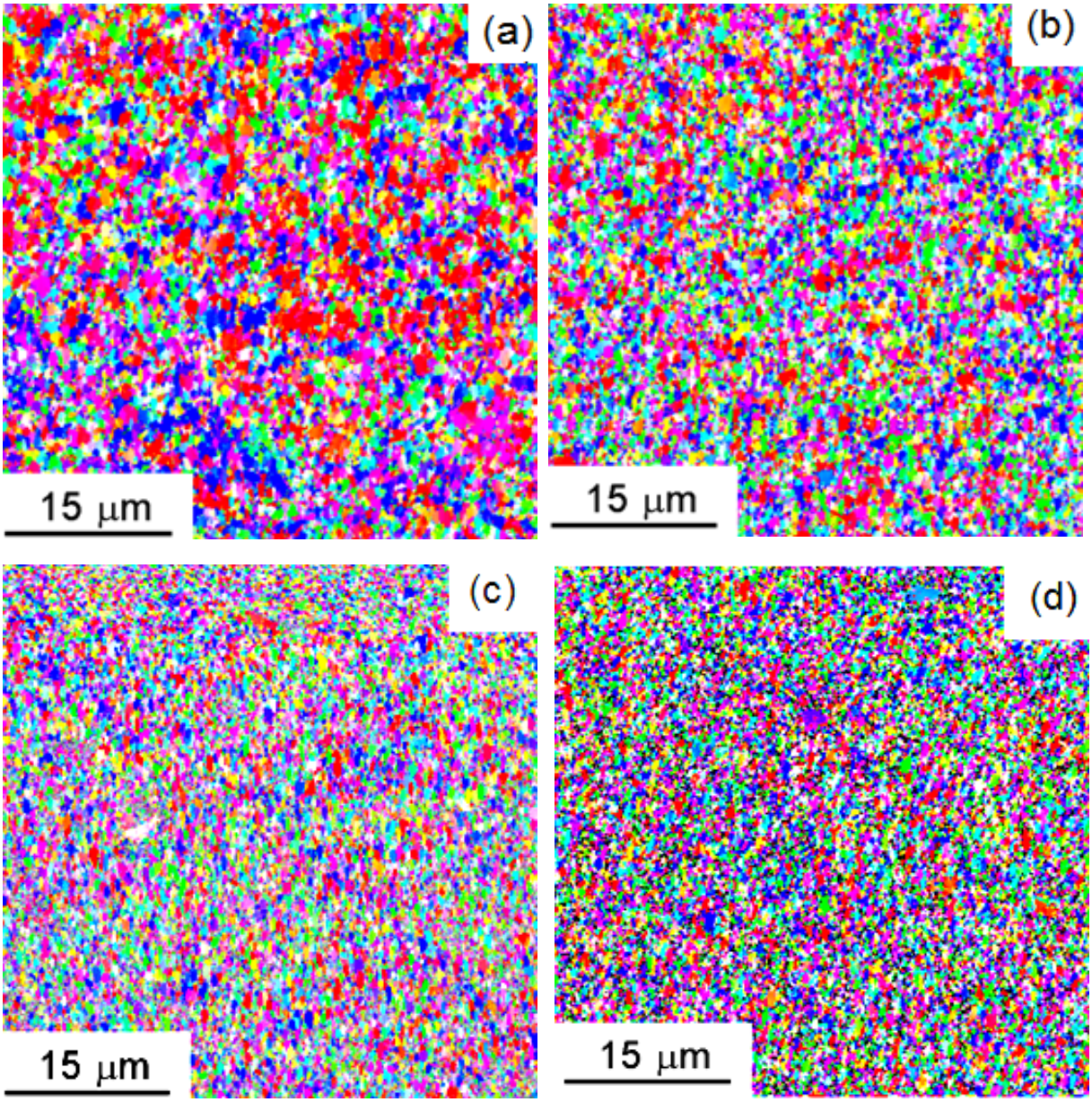

Fig. 3.3: Grain structure of alloy after (a) 1, (b) 5, (c) 10 and (d) 20 turns of HPT

To illustrate the ultrafine microstructures achieved after 10 and 20 turns, Figure 3.4 shows the QI maps measured at the disk periphery after (a) 10 and (b) 20 turns: these maps used areas of 5 μm × 5 μm and step sizes of 0.025 μm. The QI parameter, determined from the intensity of the peaks detected in the Hough space, permits a direct characterization of the quality of the Kikuchi pattern for any selected point on the map. Thus, a good pattern within a recrystallized grain requires that the corresponding point is colored close to white. By contrast, if the beam is focused on a boundary then the point has a dark color close to black. A grey level is used between these two limits and this makes it possible to build up the microstructure. Figure 3.4 (a) and (b) demonstrates a very high level of grain refinement at

the periphery of the disks after 10 and 20 turns. As noted in table 3.1, there was also significant grain refinement in the centers of the disks after 10 and 20 turns.

Table 3.1: Average grain sizes of the Al–0.6% Mg–0.4% Si alloy processed by HPT.

Number of turns	Grain size (nm)		
	Center	Mid-radius	Edge
1	1050	720	580
5	600	580	550
10	310	250	240
20	280	250	250

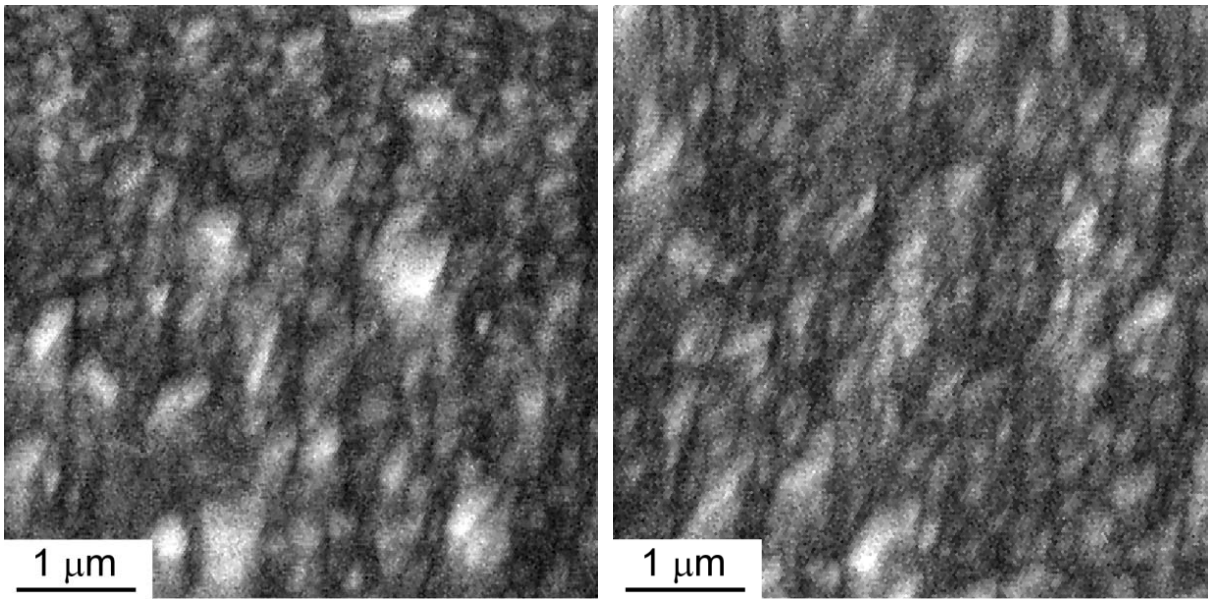

(a) **(b)**

Fig. 3.4: Quality index maps for the alloy processed through (a) 10 and (b) 20 turns of HPT.

2.2 Evolution of the grain boundary misorientation during HPT

The misorientation between the grains was measured using EBSD and the results are shown in Fig. 3.5 for the distributions at the mid-radius position after processing through 1, 5, 10

and 20 turns. These distributions show the large fraction of low angle grain boundarie LAGBs (< 15°) presents in the sample processed by 1 turn and achieved a value in the vicinity of 53 %. The subsequent evolution towards higher angles of misorientations with increasing numbers of turns is observed. The fractions of high-angle grain boundaries (HAGBs) recorded after processing trough 5 turns is similar to those reported for other materials such as commercial purity Al *[Zhilyaev et al., 2007],* Al-6061 *[Loucif et al., 2010],* and high-purity Ni *[Zhilyaev et al., 2002; 2005; 2007]*. For example, in Al-6061 alloy the fraction of HAGBs was measured as ~65% after HPT through 5 turns at a pressure of 6.0 GPa *[Loucif et al., 2010]* whereas the present tests give a fraction of HAGBs of ~61% after HPT under the same processing conditions.

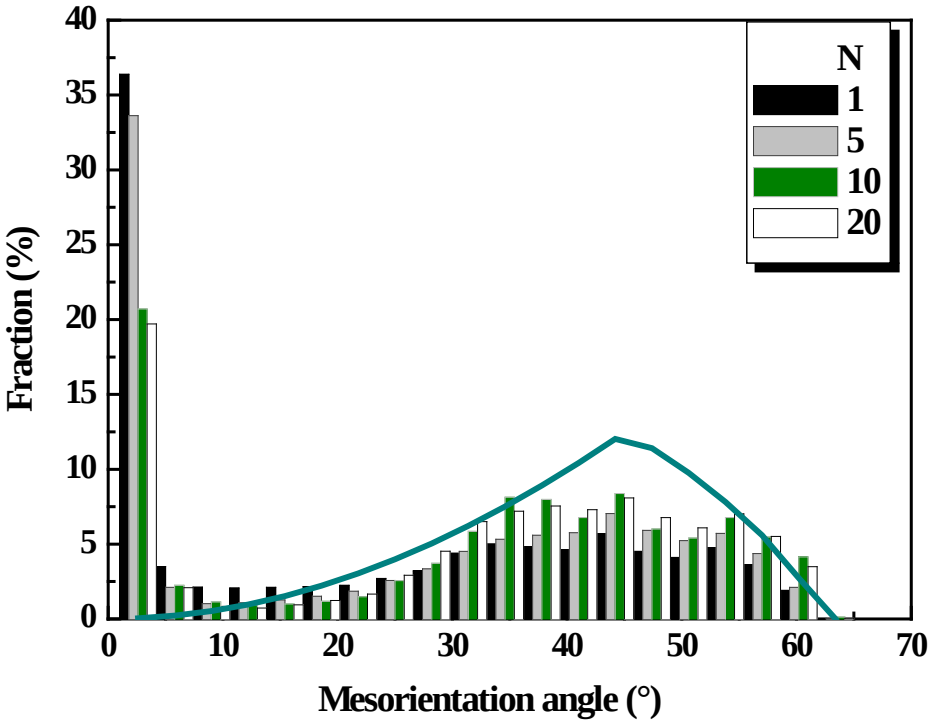

Fig. 3.5: Distributions of the misorientation angles fraction of the grain boundaries at the mid-radius of disks processed through 1, 5, 10 and 20 turns of HPT.

The fraction of high angle grain boundaries HAGBs (>15°) after 10 and 20 turns achieved the values in the vicinity of 74 % and 75 % respectively and the distributions of misorientations after 10 and 20 turns of HPT tends to evolve near the theoretical random distribution which is shown by the solid curve in Fig. 3.4 *[Mackenzie, 1958; Pippan et al., 2006].*

2.3 Evolution of hardness during HPT

The Vickers microhardness, Hv, was recorded along diameters of each disk after processing through 1, 5, 10 and 20 turns and plotted in Fig. 3.6 versus the distance from the center of each disk: the lower broken line shows the initial hardness for the material after the solid solution treatment. In the unprocessed condition, the average value at hardness is about Hv=70. Careful inspection of these plots shows the hardness increases significantly at the edge of the disk from Hv≈ 70 to Hv ≈ 142 after one turn but in the center of the disk the increase is only to Hv≈ 108. After larger numbers of turns the hardness becomes more homogeneous across the disk radius and after 10 and 20 turns the hardness values are reasonably constant at Hv ≈ 155.

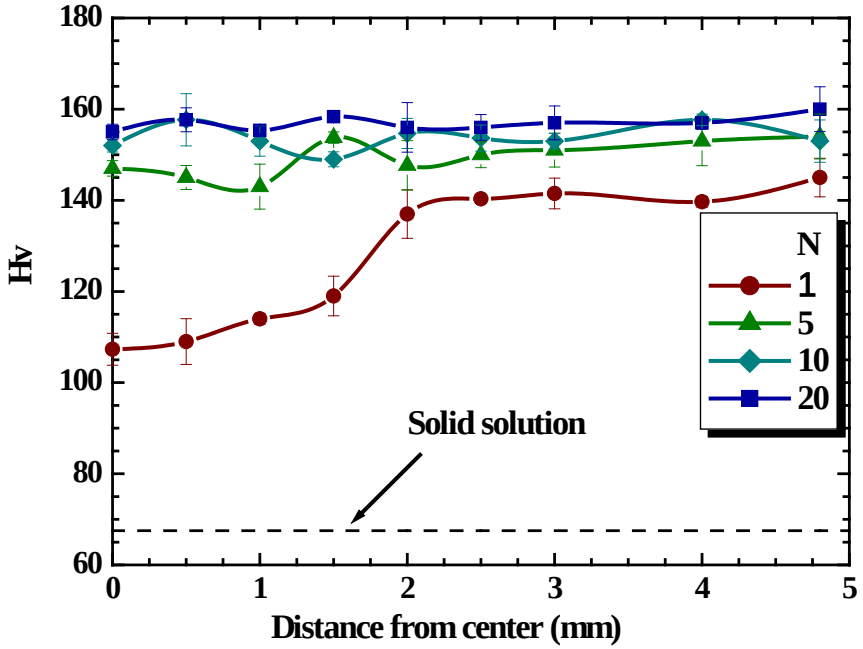

Fig. 3.6: Variation of hardness with distance from the center of the disk for samples processed by HPT through different numbers of turns.

It was noted in an earlier HPT processing of an austenitic steel that the variation in the measured hardness values with distance from the center of each disk may be reasonably correlated by replotting the datum points in terms of the equivalent strain ***[Vorhauer and Pippan, 2004]***. More recently, this approach has been used successfully with several different materials processed by HPT ***[Harai et al., 2008; Edalati et al., 2008; Ito and Horita, 2009; Kawasaki et al., 2010; Xu et al., 2010].*** The equivalent strain imposed on each disk was given earlier in equation 1.3. Using this relationship, the hardness values are re-plotted in Fig. 3.7 against the calculated equivalent strain using the procedure first suggested in the early HPT

processing of an austenitic steel *[Vorhauer and Pippan, 2004]*. These results show that the hardness values saturate at Hv ≈ 158 at all values of the equivalent strain above ~100.

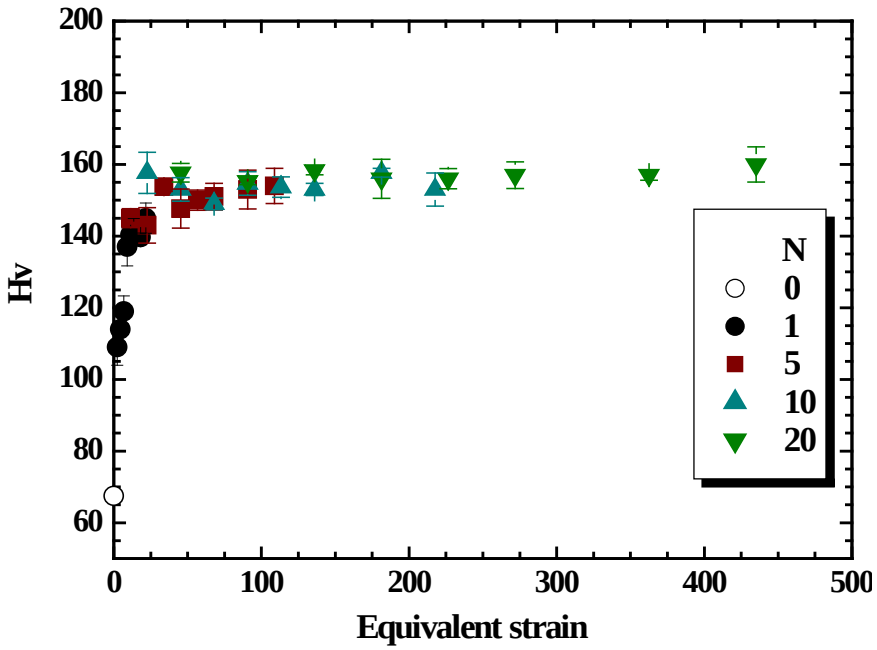

Fig. 3.7: Evolution of hardness as a function of the equivalent strain imposed by HPT.

2.4 Microstructure evolution of aging disks

In order to evaluate the effect of aging treatment on the mictrostructure evolution with HPT turns, set of the disks are aged at 473 K and 523 K for 5 minutes after solid solution. The EBSD observations are taken in the mid-radius of the discs processed after 1, 5 and 20 complete revolutions. The EBSD maps shown in the Fig. 3.8 depict the microstructures of the aged samples at 473 K alloy processed by HPT through (a) 1, (b) 5 and (c) 20 turns. These images reveal a little development of the microstructure after 1 turns. Indeed, the average grain sizes are about 600, 450 and 350 nm after 1, 5 and 20 turns respectively. These grain sizes after 1 and 5 turns are smaller than in the solution-treated alloy by a factor of about 1.2 and 1.3 respectively. However, after 20 turns the average grain size is a little larger.

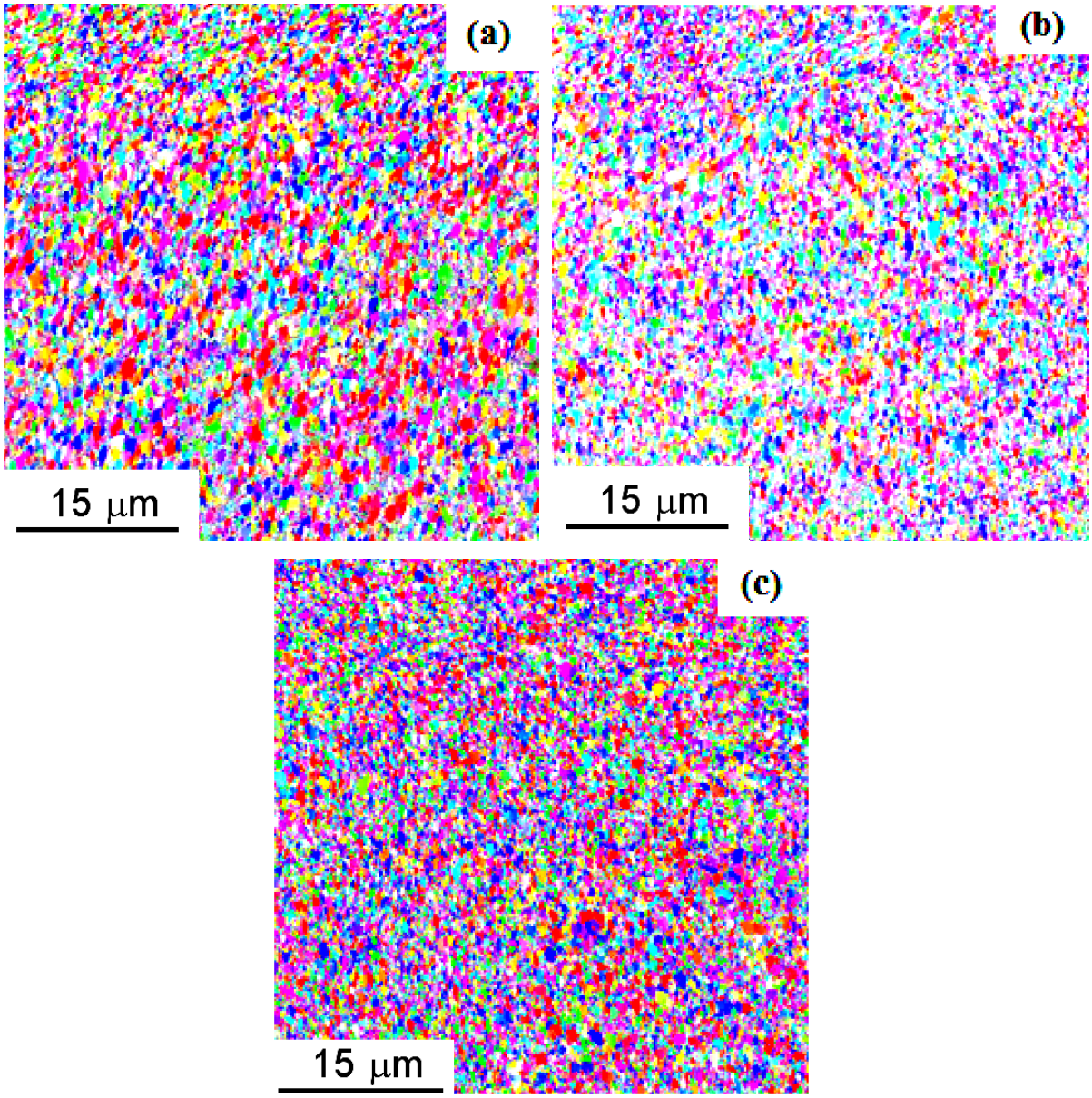

Fig. 3.8: EBSD maps: Grain structures of the aged alloy at 473K after HPT processing through (a) 1, (b) 5 and (c) 20 turns

A similar set of images is shown in Fig. 3.9 for the aged alloy at 523K processed by HPT through (a) 1, (b) 5 and (c) 20 turns. The grain size is slightly larger than in the solution-treated alloy and after 20 turns is ~400 nm.

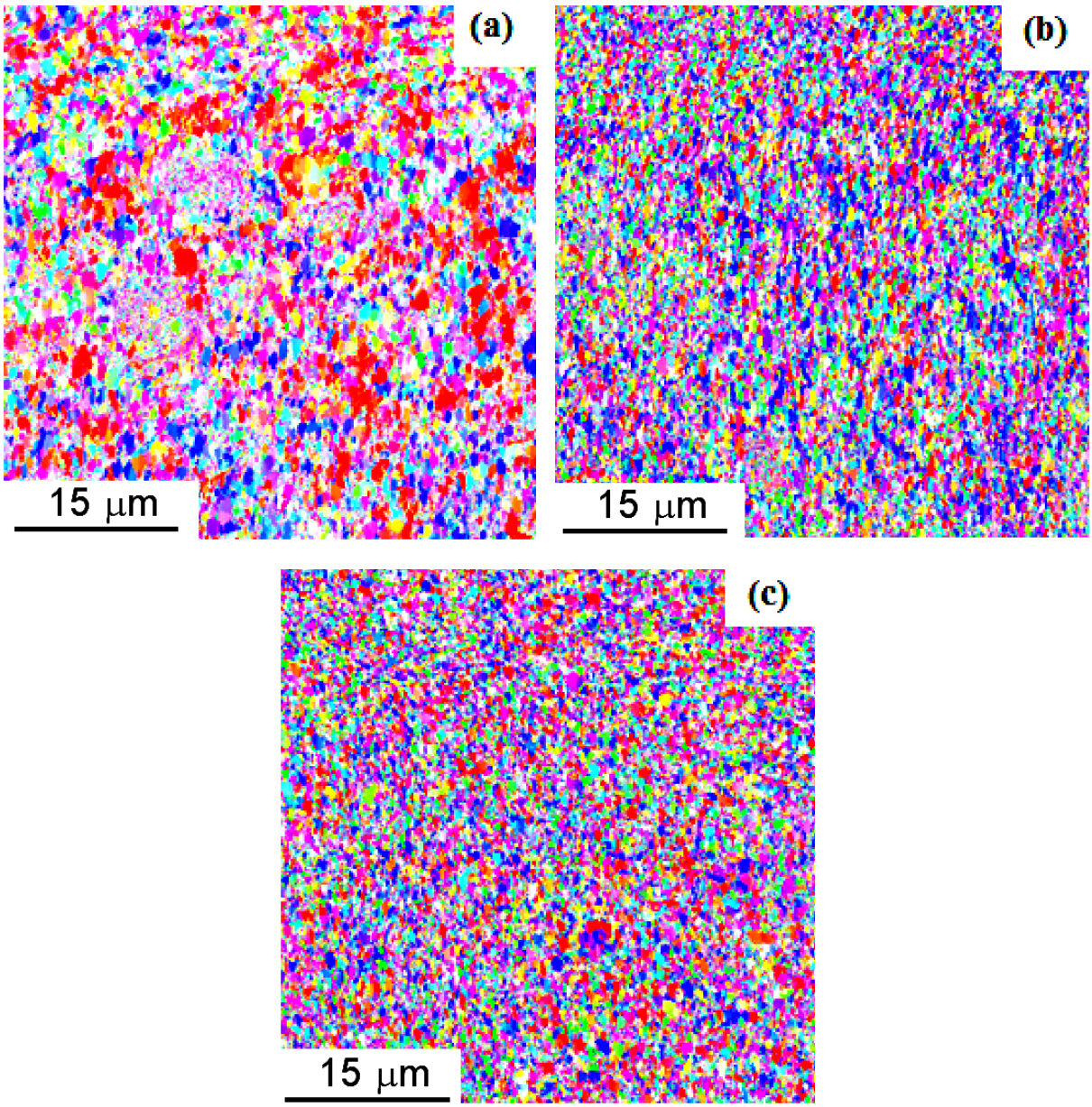

Fig. 3.9: *EBSD maps: Grain structures of the aged at 523K alloy after HPT processing through (a) 1, (b) 5 and (c) 20 turns*

The fraction of high-angle grain boundaries (HAGBs) is shown in Fig. 3.10 as a function of the number of HPT turns for the solution-treated alloy and the alloy subjected to aging at 473 K and 523 K respectively. For these conditions, the fraction tends to increase with increasing torsional straining although for the aged condition is less important between 5 and 20 turns. After 20 turns the fractions of HAGBs are ~76%, ~68% and ~74% in the solution-treated and aged at 473 and 523 K conditions, respectively. The fractions of HAGBs are quite similar in both conditions with ~76% of HAGBs in the solution-treated alloy and ~68% in the aged condition. These fractions are consistent with other results reported for materials processed by HPT such as ~65-67% of HAGBs for high-purity Ni ***[Zhilyaev et al., 2003]***. They are also

comparable with fractions of HAGBs reported for materials processed by ECAP through large numbers of passes, such as ~74% in high-purity Al *[Kawasaki et al., 2009]* and ~65% in an Al-1% Mg solid solution alloy *[Xu et al., 2011].*

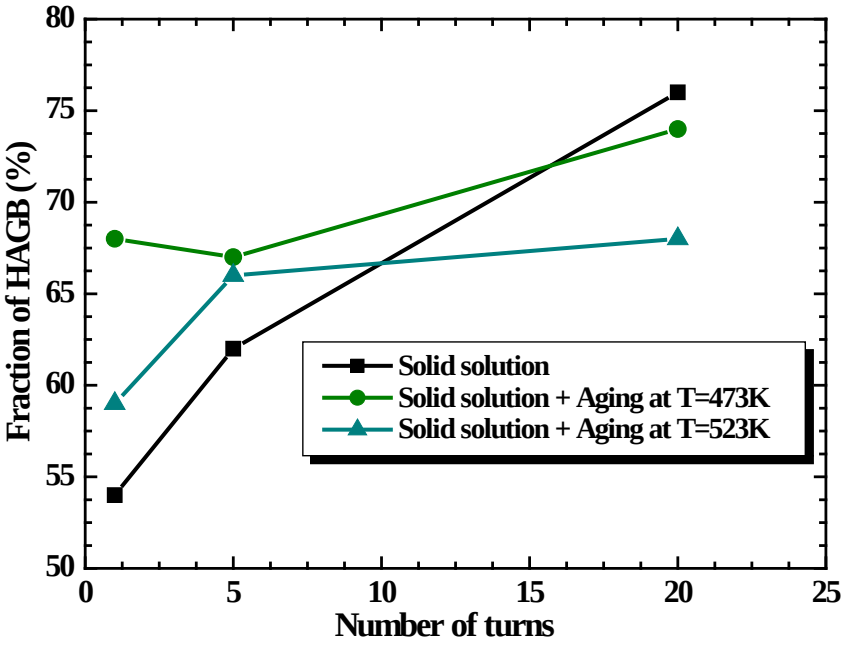

Fig. 3.10: Fraction of high-angle grain boundaries versus number of turns in HPT processing for the solution-treated and aged conditions.

2.5 Influence of HPT temperature on the microstructure

The disk was processed by HPT under quasi-constrained conditions at temperature of 373 K Heating of the samples to 373 K was achieved using heating elements embedded in the upper and lower anvils, and the temperature was controlled using a thermocouple placed within the upper stationary anvil. The time for heating to 373 K was~15 minutes, and thereafter, the temperature was held constant during HPT processing to a temperature within the range of 373± 5 K. The microstructures taken at the mid-radius after 5 turns processing at room and at 373K are represented in Fig. 3.11. This figure shows no appreciable change in the microstructure and the grain size is about 580 nm in the both conditions.

The distribution of misorientations between the grains of the disks processed at room temperature and at 373K is depicted in Fig. 3.12. These distributions exhibit the same profile and present just little difference of the fraction of high angle. Indeed, these fractions are respectively 61 and 68 %. Then the temperature has only a little influence on the microstructures.

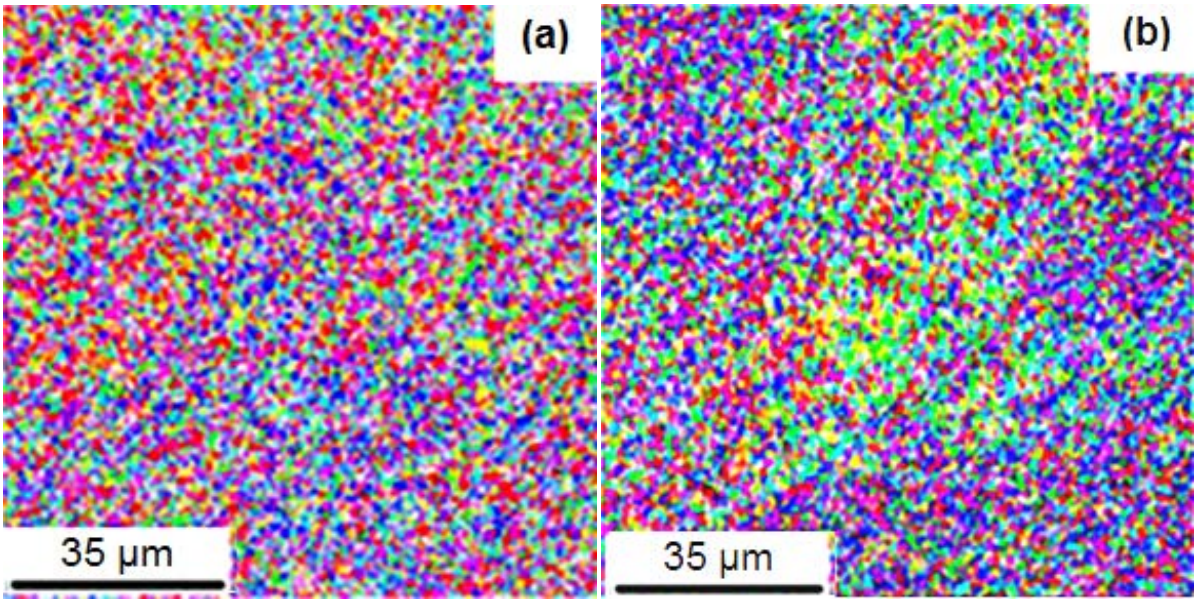

Fig. 3.11: EBSD maps after 5 turns HPT processing at (a) room temperature and (b) 373K.

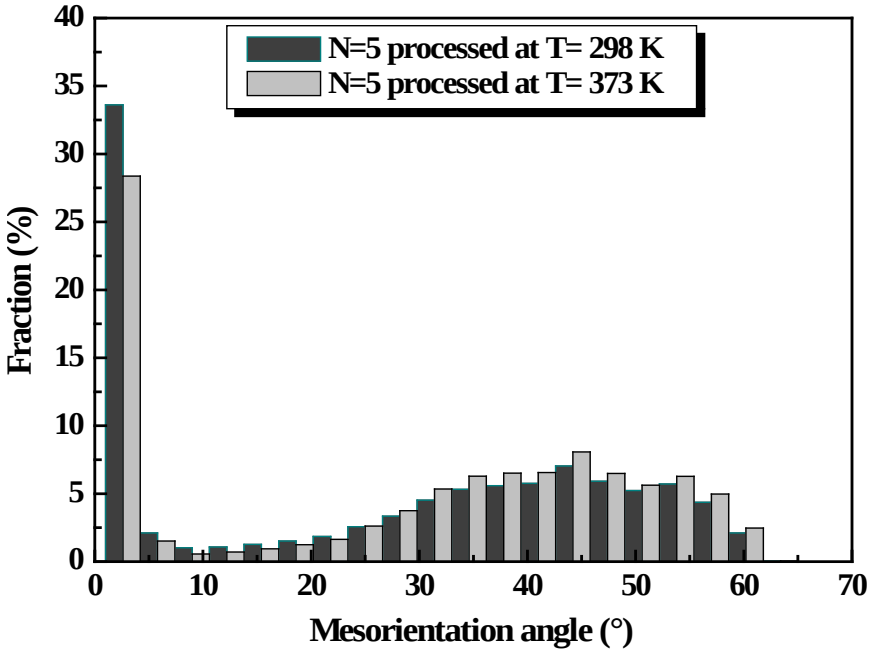

Fig. 3.12: Distributions of the misorientation angle fraction of the grain boundaries at the mid-radius of disks processed in terms of the HPT temperature for 5 turns.

3. Microtexture evolution

3.1 Microtexture of the alloy in initial state of solid solution

The microtexture evolution with HPT deformation was determined by means of ODF analysis. It is presented as plots of constant φ_2 = 45° sections where these sections are calculated using the harmonic series expansion with a series rank of 22 and Gaussian smoothing of 5°. The texture of the unprocessed (initial solid solution) sample is taken across the disc with the step size of 5μm and shown in the Fig. 3.13. The texture is almost random and the ODF maximum value is 2.3.

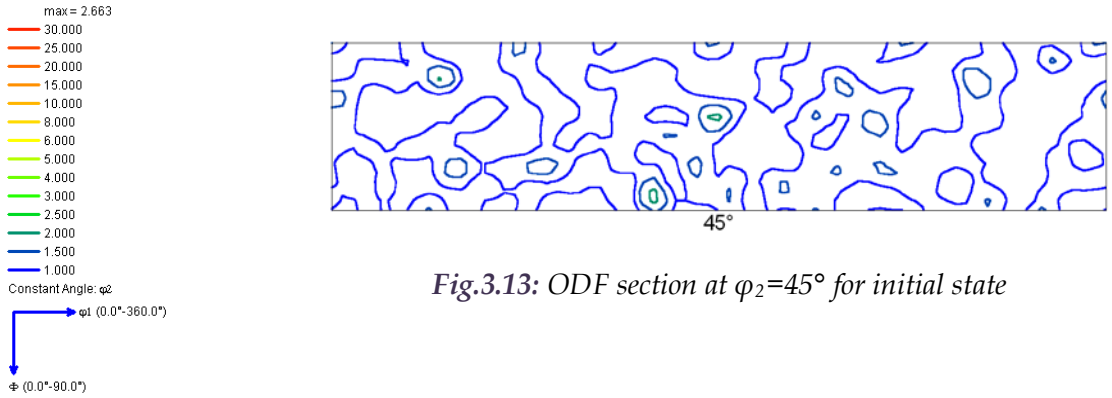

Fig.3.13: ODF section at φ_2=45° for initial state

The evolution of HPT texture versus number of turns is shown in Fig. 3.14 (a-d) and can be interpreted with the aid of the key given in Fig. 3.14 (e) which shows the positions of the ideal texture components. Each measurement was taken at the mid-radius covering an area of 100 × 100 μm², mapped with a step size of 0.1 μm. After 1 turn (Fig. 3.14a), the C component develops preferentially and exhibits a f (g) max value of 5.7. Furthermore, the presence of weak A* and A components is observed When the deformation increases, the C component is still present but to a lesser extent. For N = 5 turns, there also appears a new component, generally not mentioned in the literature, which is close to {110} <221> (φ_1 = 160° and 340° ϕ = 90°, φ_2 = 45°). No significant change in the texture sharpness was observed in this study with excessive deformation and this is attributed to the occurrence of dynamic recovery. Note also that size (statistic) and positioning exact location as regard to the torsion experiments) of scan areas may cause errors in the interpretation of textures. With increasing number of turns an overall tendency towards a weakening and randomization is clear after 20 turns.

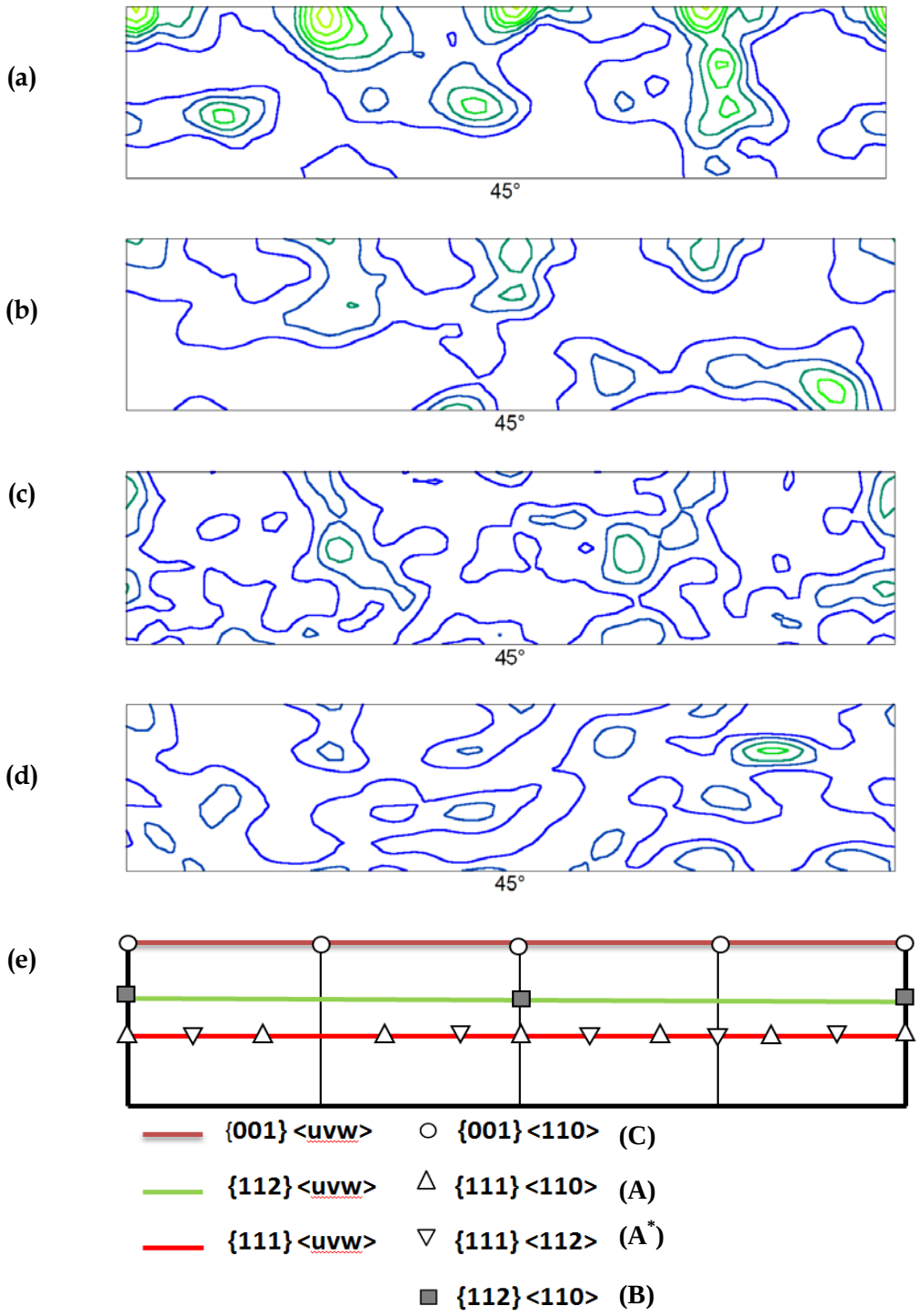

Fig. 3.14: ODF sections at φ_2=45° after (a)-(d) 1, 5, 10 and 20 HPT turns and (e) position of the ideal texture components.

The evolution of texture during monotonous HPT was studied earlier in pure aluminum *[Orlov et al., 2009].* This study revealed that the deformation texture varies in a systematic manner with increasing strain. With increasing strain, the intensity of the A component

decreases while the C orientation becomes stronger. With further increase in strain, the volume fraction of the C component decreases and the texture is found to be weakened and randomized. Major texture maxima corresponding to the C component were observed for ECAP, HPT and ECAP+HPT nickel samples subjected to a total of 5 complete revolutions at room temperature under an applied pressure of 6 GPa ***[Zhilyaev et al., 2004].***

3.2 Microtexture evolution after HPT processing and aging

The effect of aging treatment at 473 K and 523 K on the microtexture was examined and the ODF sections are represented in figures 3.15 and 3.16 respectively together with the aid of the key given which shows the positions of the ideal texture components. Careful inspection of the ODF section of the disks aged at 473 K after 1 turn reveals the appearance of the torsion texture components presented in sample processed in the solid treated condition after one turn (Fig. 3.15a) with the presence of the weak A^* and A components. These components develop and get sharpened After 5 turns. The A^* get also sharpened while the initial strong C component is manifestly weakened after 20 complete revolution.

The ODF sections after ageing at 523 K are depicted in Fig. 3.16. The C component develops after 1 turn (Fig. 3.16a) with the high f (g) max compared with the solid treated and aging at 473 conditions. With increasing number of turns, the weakening of the C component is observed and only a remnant A component is manifestly present. An overall tendency towards a randomization is clear after 20 turns.

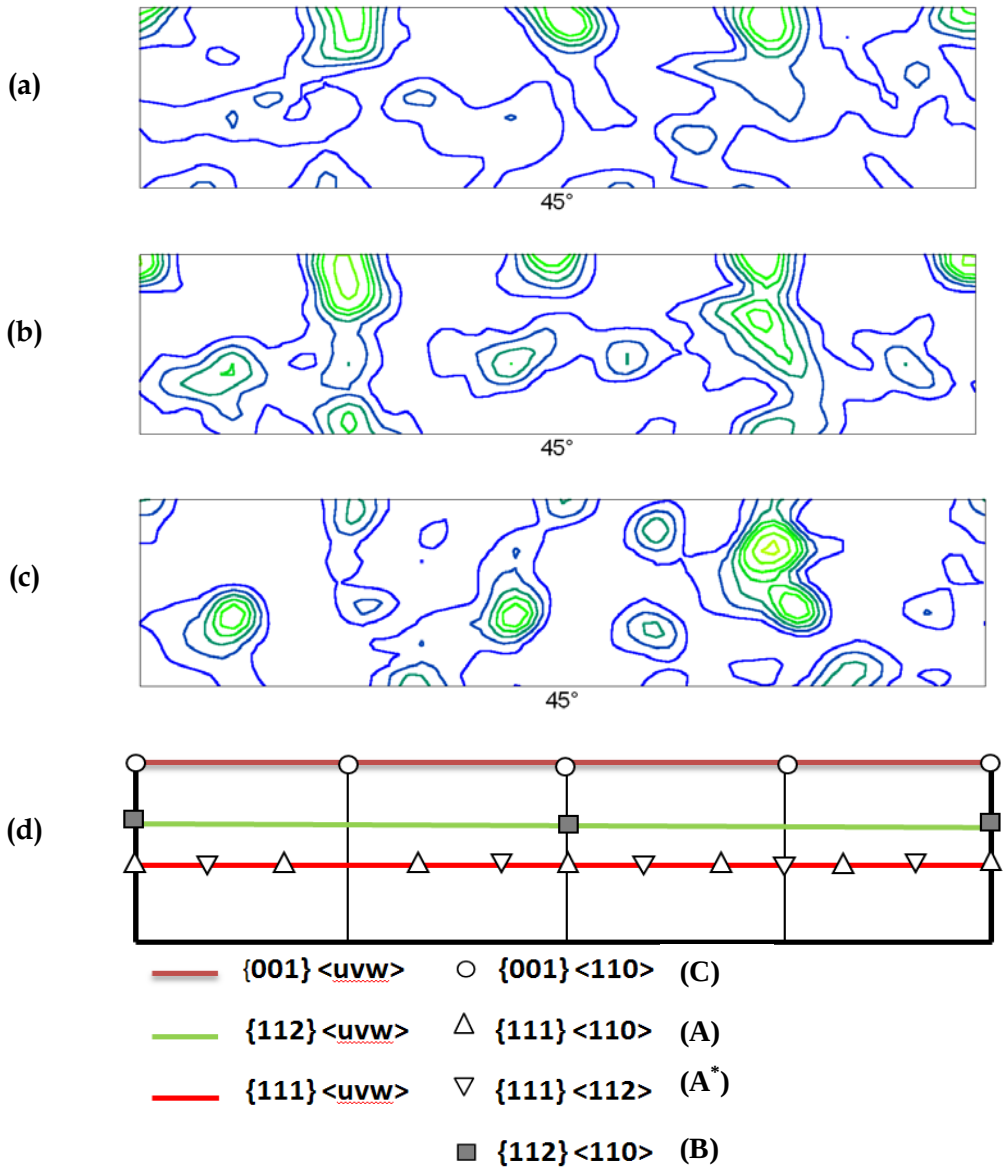

Fig. 3.15: ODF sections at φ_2=45° of aged samples at 473 K after (a)-(d) 1, 5 and 20 HPT turns and (e) position of the ideal texture components.

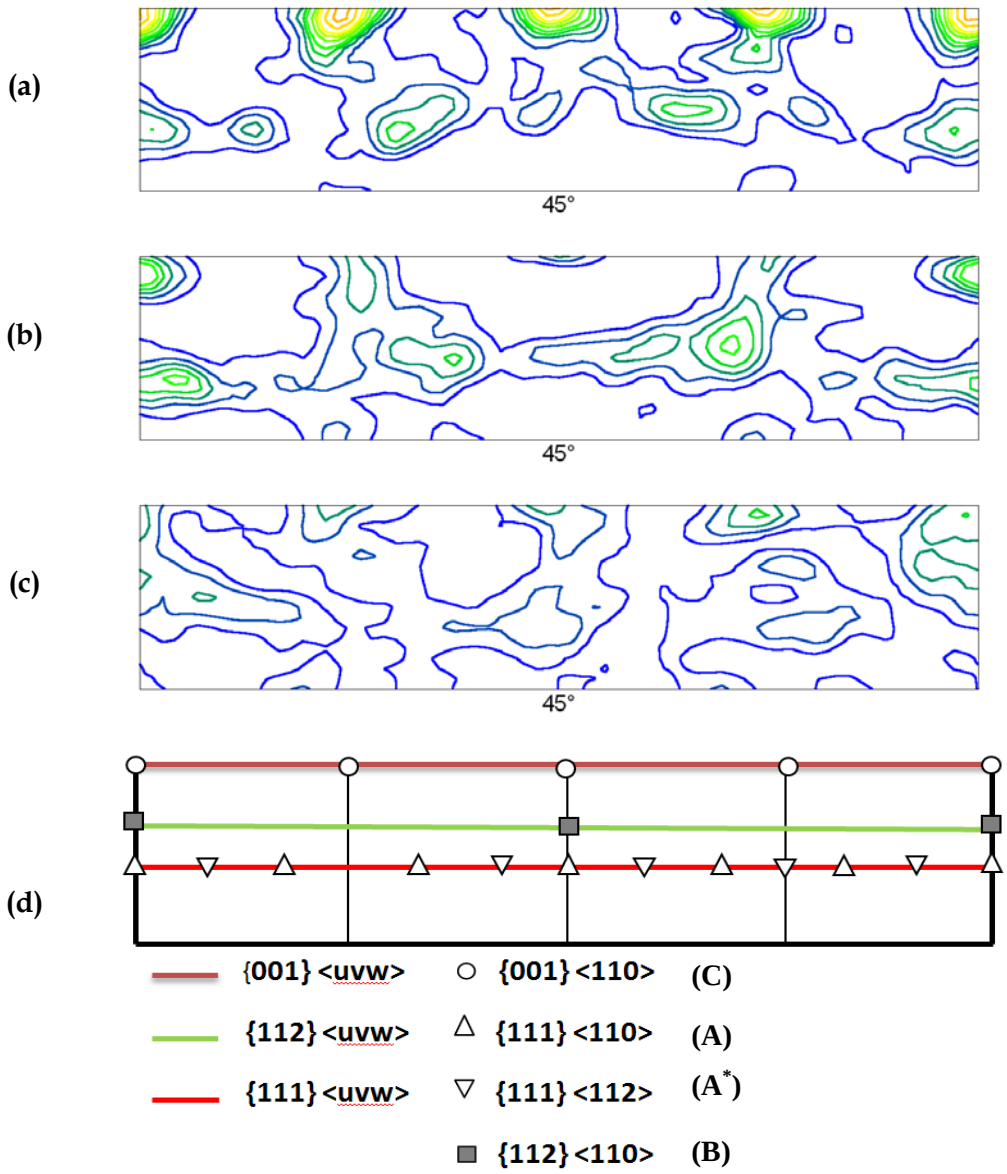

Fig. 3.16: ODF sections at φ_2=45° of aged samples at 473K after (a)-(d 1, 5 and 20 HPT turns and (e) position of the ideal texture components.

The graph plotted in the Fig. 3.17 presents the variation of the f (g) max against the number of turns for the three conditions of the disk (unprocessed and aged at 473 and 523 K) subjected up to 20 complete revolutions. This figure shows a decrease of the maximum after 1 turn for both solid-treated samples and aged at 523 K. The higher value of f (g) max recorded at the sample aged at 523 K is probably due to the statistical problem mentioned above. The f (g) max is quite unchanged with further straining for sample aged at 473 K and presents a value in the vicinity of 5.

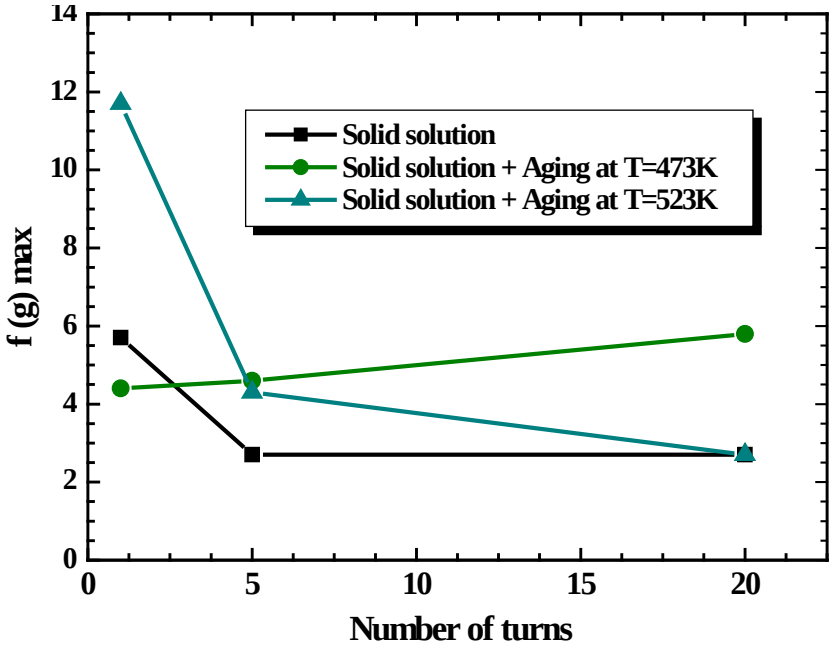

Fig. 3.17: Maximum density of ODF section versus number of turns of the solid-treated and aged sample

4. Conclusion

It is shown that processing by HPT up to 20 complete revolutions leads to microstructural refinement with an average grain size of ~250 nm, high fraction of high-angle grain boundaries of about 74% and to an increase in hardness up to a saturation value at equivalent strains above ~100. An ODF analysis revealed an initial texture that was near random and the development of an ideal torsion texture during HPT processing in particular the C {001}<110> component, tended to develop.

References

Edalati K., Fujioka T., Horita Z., Mater. Sci. Eng. A 497 (2008) 168.

Furukawa M., Horita Z., Nemoto M., Valiev R.Z., Langdon T.G., Phil. Mag. A 78 (1998) 203.

Harai Y., Ito Y., Horita Z., Scripta Mater. 58 (2008) 469.

Ito Y., Horita Z., Mater. Sci. Eng. A 503 (2009) 32.

Kawasaki M., Ahn B., Langdon T.G., Acta Mater. 58 (2010) 919.

Kawasaki M, Horita Z, Langdon TG Mater Sci Eng A524 (2009) 143

Loucif A., Figueiredo R.B., Baudin T., Brisset F., Langdon T.G., Mater. Sci. Eng. A 527 (2010) 4864.

Mackenzie J.K., Biometrika 45 (1958) 229.

Orlov *D., Bhattacharjee P. P., Todaka Y., Umemoto M., Tsuji N., Scripta Mater. 60 (**2009**) 893.*

Pippan *R., Scheriau S., Taylor A., Hafok M., Hohenwarter A, Bachmaier A., Ann. Rev. Mater. Res. 40 (**2010**) 319.*

Pippan *R., Wetscher F., Hafok M., Vorhauer A., Sabirov I., Adv. Eng. Mater. 8 (**2006**) 1046.*

Sakai *G., Horita Z., Langdon T.G., Mater. Sci. Eng. A 393 (**2005**) 344.*

Skinner *D. J., Bye R. L., Raybould D., Scripta Met. 20 (**1986**) 867-872.*

Vorhauer *A., Pippan R., Scripta Mater. 51 (**2004**) 921.*

Xu *C., Horita Z.,Langdon T.G., Acta Mater. 55 (**2007**) 203.*

Xu *C., Horita Z, Langdon T.G., Acta Mater. 56 (**2008a**) 5168.*

Xu *C., Horita Z., Langdon T.G., Mater. Sci. 43 (**2008b**) 7286.*

Xu *C., Horita Z., Langdon T.G., Mater. Sci. Eng. A528 (**2011**) 6059.*

Xu *C., Horita Z., Langdon T.G., Mater. Trans. 51 (**2010**) 2.*

Xu *C., Langdon T.G., Mater. Sci. Eng. A 503 (**2009**) 71.*

Zheng *J. G., Vincent R., Steeds J. W., Phil. Mag. 80 (A) (**2000**) 493-500.*

Zhilyaev *A. P., Baró M. D., Langdon T. G., McNelley T. R., Rev. Adv. Mater. Sci. 7 (**2004**) 41.168.*

Zhilyaev *A.P., Kim B.K., Nurislamova G.V., Baró M.D., Szpunar J.A., Langdon T.G, Scripta Mater. 46 (**2002**) 575.*

Zhilyaev *A.P., Kim B.K., Szpunar J.A., Baró M.D., Langdon T.G, Mater. Sci. Eng. A 391 (**2005**) 377.*

Zhilyaev *A.P., Lee S., Nurislamova G.V., Valiev R.Z., Langdon T.G., Scripta Mater. 4 (**2001**) 2753.*

Zhilyaev *A.P., McNelley T.R., Langdon T.G., Mater. Sci. 42 (**2007**) 1517.*

Zhilyaev *A.P., Nurislamova G.V., Kim B.K., Baró M.D., Szpunar J.A., Langdon T.G., Acta Mater. 51 (**2003**) 753.*

Chapter 4

Mechanical Properties after HPT

1. Introduction

This chapter is initiated to evaluate the strength of our sample at room temperature which is estimated in terms of the relation between Vickers microhardness and grain size. Furthermore, the microtensile tests are used to study the mechanical properties evolution at high temperature. The accent was also placed on examining the effect of processing the alloy on mechanical properties either as a solid solution or after an aging treatment at 473 K and 523K.

2. Mechanical behavior of HPT metals at room temperature

2.1 Introduction

It is well established that the mechanical behavior of crystalline solids at low temperatures, below ~$0.5T_m$ where T_m is the absolute melting temperature of the material, is dependent upon the Hall–Petch relationship where the yield stress, σ , is given by ***[Hall, 1951; Petch, 1953].***

$$\sigma = \sigma_o + k_y d^{-1/2} \qquad (4.1)$$

Where σ_o is a friction stress, k_y is a constant of yielding and d is the grain size. From this relationship, it is readily apparent that the yield stresses of materials processed by HPT should be very high because of their extremely small grain sizes. Very little information is available at present to provide any detailed documentation of the validity of the Hall–Petch relationship when testing HPT specimens of different materials. The reason for this deficiency lies in the nature of the HPT samples. The disks used in conventional HPT are very small and therefore, although there are many reports describing measurements of hardness in these materials, there are only a very limited number of reports describing the nature of the stress–strain curves and the mechanical behavior when testing in tension. In practice, the Hall–Petch relationship may be conveniently rearranged in terms of the Vickers microhardness *[Furukawa et al., 1998]* and this permits a simple but indirect verification of the relationship. There are several reports using this approach with hardness measurements *[Oh-Ishi et al., 1999; Sergueeva et al., 2001; Balogh et al., 2008; Zhilyaev et al., 2008].*

2.2 The significance of the Hall–Petch relationship in HPT processing

The present results reveal a clear duality in behavior. Whereas the hardness values saturate after equivalent strains of ~100 as shown in Fig. 4.1, the average grain sizes in the center of the disks recorded in Table 1 continues to decrease even up to N = 20 turns although the grain size at the mid-radius and edge positions are stable after 10 turns. To check this apparent dichotomy, the strength was estimated by taking the average of the individual hardness values at the center, mid-radius and edge of each disk, converting the units from kgf mm^{-2} to MPa, setting the flow stress, equal to Hv/3 *[Furukawa et al., 1998]* and plotting the stress as a function of the estimated average grain size, d, for these three positions as shown in Fig. 4.1. Also included in Fig. 4.1 are experimental datum points from an earlier report for the Al-6061 alloy processed at P = 6.0 GPa to a maximum of 5 turns *[Loucif et al., 2010]* and a single datum point from experiments on an Al-6061 alloy of Al–0.8% Mg–1.2% Si where processing by HPT was conducted through 5 turns at P = 6.0 GPa *[Nurislamova et al., 2008]:* the experimental point for the latter investigation lies at a much smaller grain size of ~100 nm because the investigation used disks having thicknesses of only 0.3 mm and with a large diameter of 20 mm. It is apparent that all experimental points in Fig. 4.1 are mutually consistent but the plot reveals a clear division into two separate trends with the transition occurring at a grain size of ~500 nm. Thus, the strength varies only slightly with grain size at

average sizes below ~500 nm but it varies with $d^{-1/2}$ at the larger grain sizes. This latter variation is consistent with the conventional Hall–Petch relationship which is given in equation 4.1.

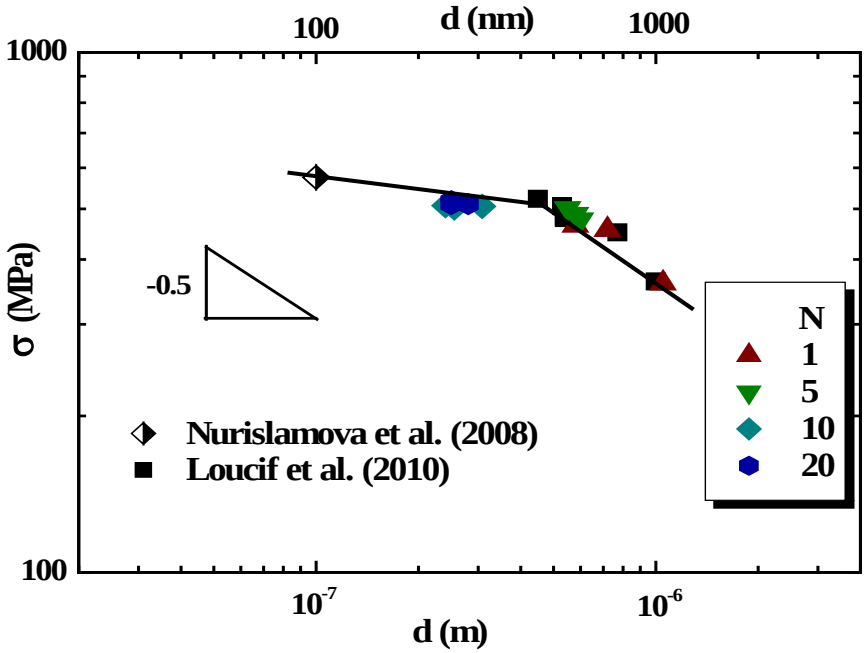

Fig. 4.1: Evolution of flow stress as a function of the average grain size after processing through 1, 5, 10 and 20 turns of HPT: data also included from Loucif et al. ***[Loucif et al., 2010]*** *and Nurislamova et al.* ***[Nurislamova et al., 2008].***

To further check on the applicability of the Hall–Petch relationship, the values of were plotted directly as a function of $d^{-1/2}$ as shown in Fig. 4.2. This plot confirms the conventional Hall–Petch relationship at larger grain sizes on the left, at $d^{-1/2} < 1500$ $m^{-1/2}$, where $\sigma_o \approx 50$ MPa and $k_y \approx 0.326$ MPa $m^{1/2}$ whereas at smaller grain sizes there is a deviation in the Hall–Petch relationship and the relevant values are $\sigma_o \approx 500$ MPa and $k_y \approx 0.011$ MPa $m^{1/2}$. A break in the standard Hall–Petch relationship is well established in nanostructured materials although the deviation usually leads to an inverse trend which occurs typically at grain sizes of ~25 nm or smaller ***[Meyers et al., 2006].*** By contrast, the deviation in Fig. 4.2 does not lead to an inverse relationship and it is present at a grain size of ~500 nm. Nevertheless, there are earlier reports of similar deviations from the Hall–Petch relationship in materials processed by HPT and ECAP. For example, a sharp deviation in the Hall–Petch relationship was observed at a grain size of ~150 nm in an Al–1.5% Mg alloy processed by HPT using a pressure of 4 GPa ***[Valiev et al., 1992]***, at grain sizes below ~150 nm in an Al–3% Mg alloy

processed by HPT using a pressure of 5 GPa *[Furukawa et al., 1996]* and at grain sizes below ~200 nm for an Al–Mg–Li–Zr alloy processed by ECAP through 4 turns *[Furukawa et al., 1997].* Al l of these results show similarities to the present data. However, the present results differ from very recent data for Ni containing a small amount of Ti where processing by HPT led to exceptionally high strength at a grain size of <50 nm *[Zhang et al., 2011].* Two explanations were proposed earlier for the breakdown in the Hall–Petch relationship at grain sizes below ~200 nm. On the one hand, it was suggested that the non-equilibrium grain boundaries introduced into the material in SPD processing are reasonably transparent to the movement of mobile lattice dislocations so that the effective grain size for the Hall–Petch relationship is larger than the measured value because the dislocations pass easily through these boundaries *[Valiev et al., 1992].*

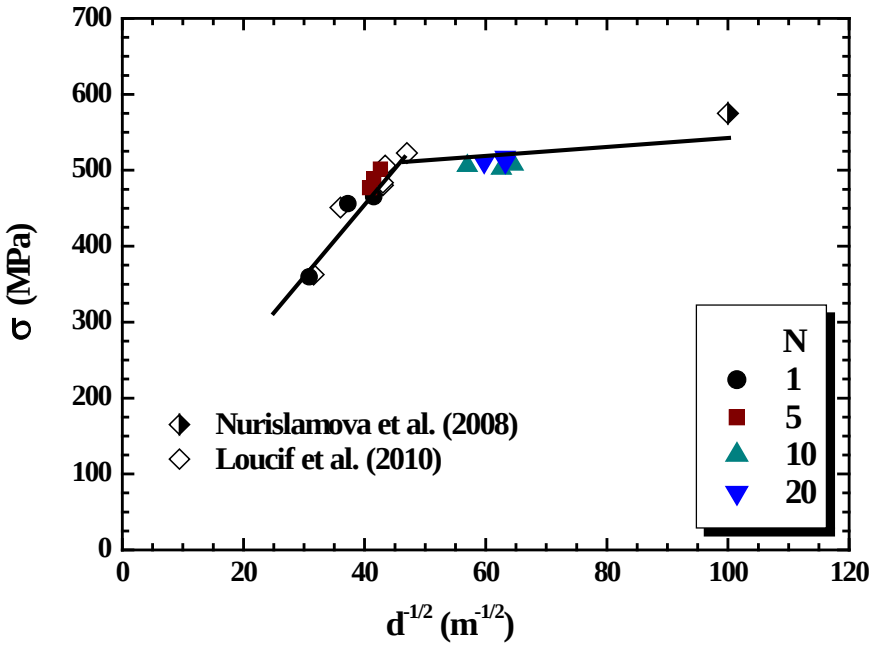

Fig. 4.2: The Hall–Petch relationship for samples processed through 1, 5, 10 and 20 turns of HPT: data also included Loucif et al. [Loucif et al., 2010] and Nurislamova et al. [Nurislamova et al., 2008].

On the other hand, it was proposed that the breakdown occurs because of the high volume fraction of grain boundaries and the increased participation of extrinsic dislocations which are able to move in the non-equilibrium grain boundaries, and thereby reduce the apparent strength, during the impingement of the hardness indenter *[Furukawa et al., 1996]*. The

latter proposal provides a reasonable explanation for the present results on the Al–Mg–Si alloy and it may be used also to explain the recent very high hardness values reported in Ni containing 0.14% Ti *[Zhang et al., 2011]* if, for example, the Ti solute inhibits the movement of extrinsic dislocations in the non-equilibrium boundaries.

3. Mechanical behavior at 813 K after HPT processing

Fig. 4.3(a) shows typical plots of engineering stress versus engineering strain for the solution-treated samples before and after processing by HPT. These curves are similar and there is no significant difference in the strength of the samples except the disc processed after 5 turns which exhibit a slight little in the maximum.

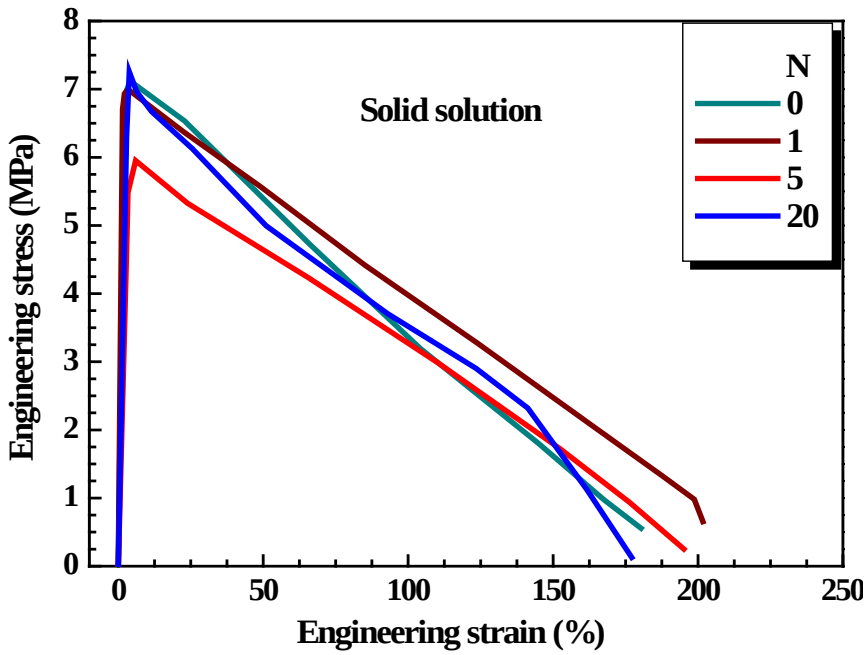

Fig. 4.3: *Engineering stress vs. engineering strain for specimens tested at 813 K after HPT processing in the solution-treated condition.*

Similar curves are shown in Fig. 4.3(b) for the samples subjected to aging at 473 K. This curve shows a little increase in the maximum with increasing number of turns. Fig. 4.3(c) show a similar curve for the samples subjected to aging at 523 K the maximum is represented at the sample processed after 1 turn. One can conclude that all of these curves are similar and there is no significant difference in the strength of the samples. This is reasonable because of the very high testing temperature.

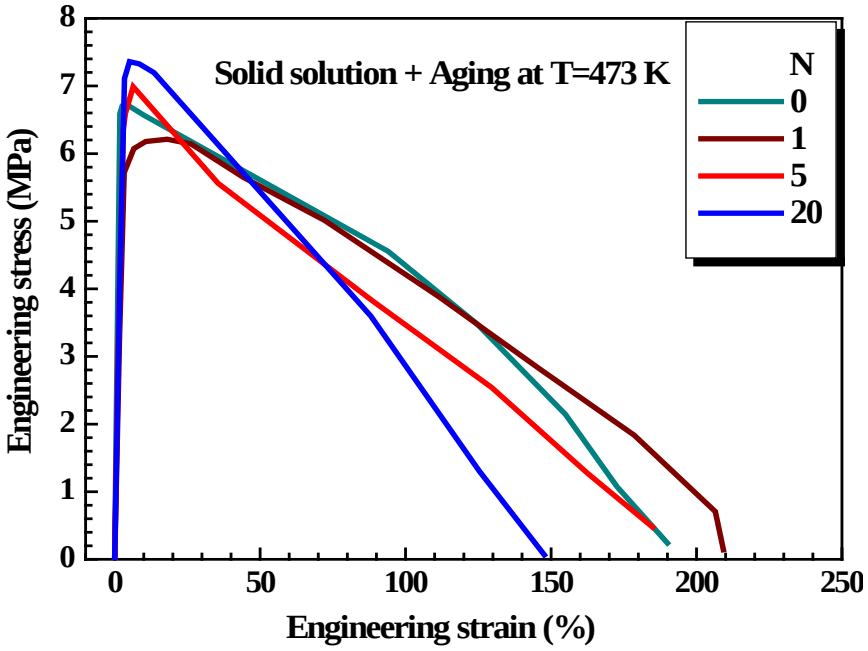

(a)

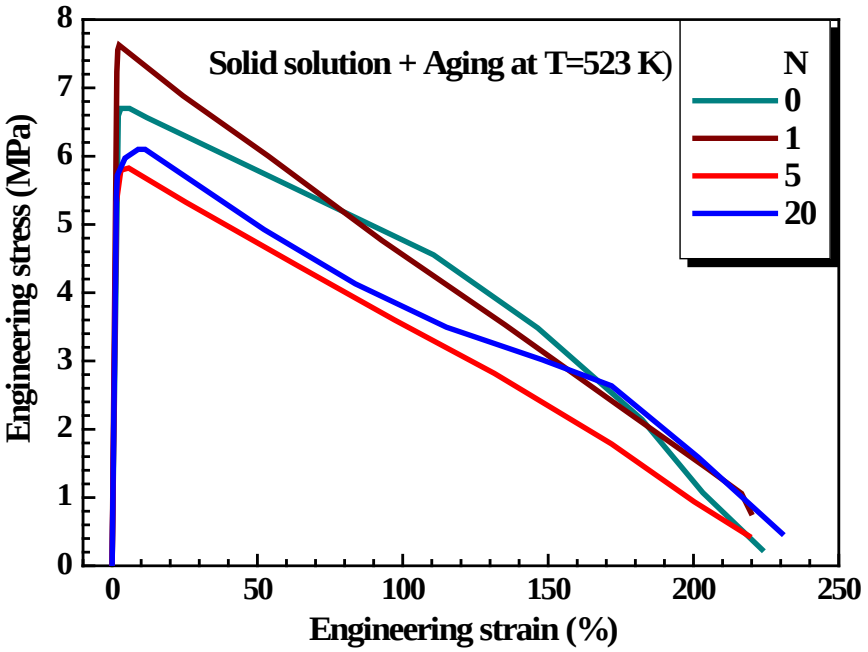

(b)

Fig. 4.4: *Engineering stress vs. engineering strain for specimens tested at 813 K after HPT processing in the aged conditions at (a) 473 K and (b) 523 K.*

The elongations to failure for these three conditions are shown in Fig. 4.5. It is apparent from these curves that the ductility of the coarse-grained unprocessed material with a grain size of 150 μm increases with the aging treatment and the elongation of failure achieved a value

from ~ 162% after solid solution to ~ 223% for the aged condition at 523 K. Aging at 473 K leads to gradually decrease in the ductility with increasing number of turns and the elongation to failure is about 220% after 1 turn to 110% after 20 complete revolutions. However, a little or no dependence on the strain introduced by HPT for the sample aged at 573 K. The aged samples are slightly more ductile than the solution-treated samples. Nevertheless, the maximum elongation of ~230% in the aged condition is not sufficient to fulfill the conditions for superplasticity which requires an elongation to failure of at least 400% *[Langdon, 2009].*

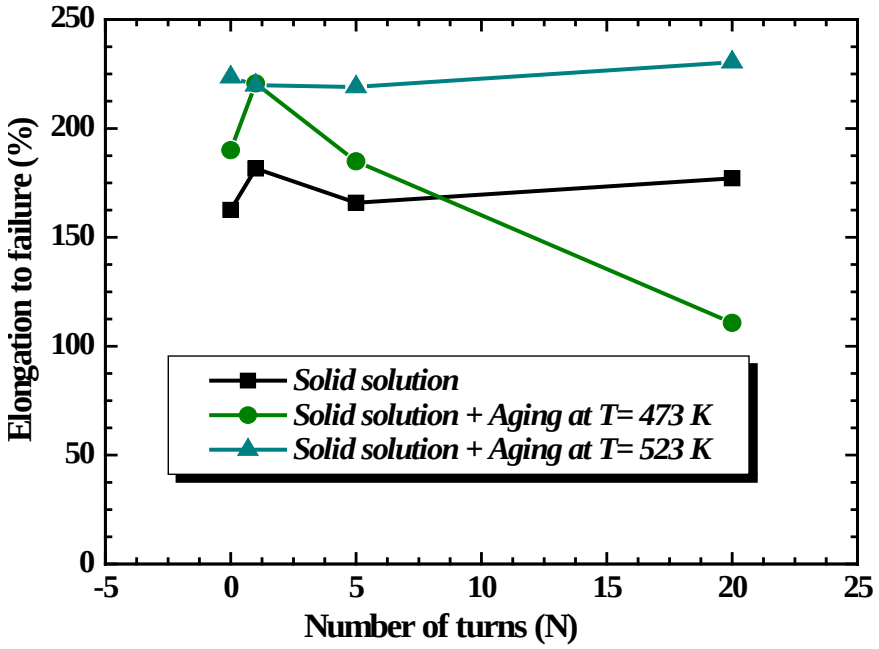

Fig. 4.5: Elongation to failure vs. number of turns in HPT processing for the solution-treated and aged conditions tested in tension at 813 K.

A more direct comparison is given in Fig. 4.6 where the yield stresses are plotted against the number of turns for the three conditions. No significant changes in the yield stresses were observed. Indeed, a little decrease in the yield stress value is occured in the aged disk at 523 K processed at 20 turns.

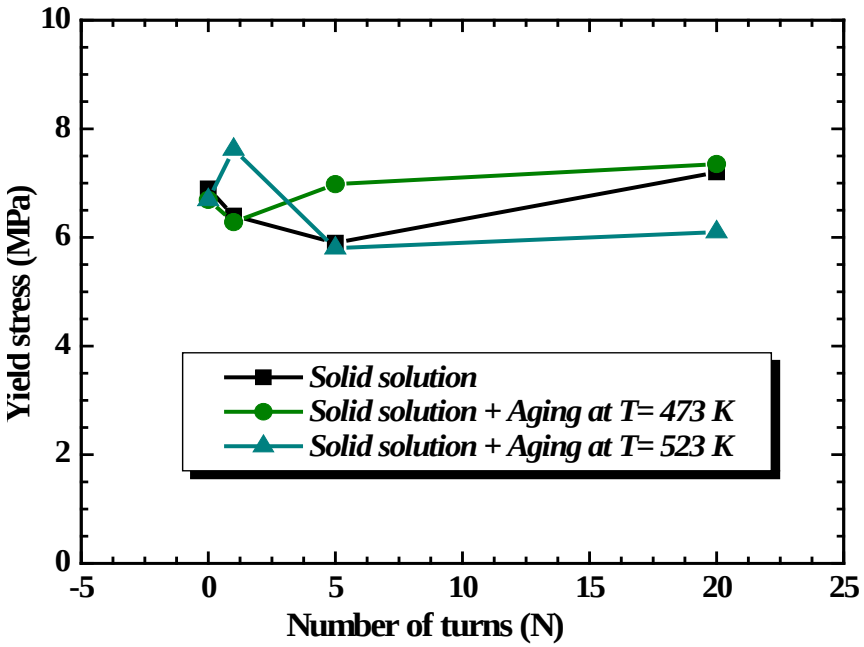

Fig. 4.6: Yield stress vs. number of turns in HPT processing for the solution-treated and aged conditions tested in tension at 813 K.

4. Conclusion

The results presented in this chapter show that the mechanical testing at a temperature of 813 K gave similar stress-strain curves and no significant difference in the strength of the samples either after solid solution and aging conditions. Aging at 523 K leads to the maximum recorded elongations to failure of ~230% which is not within the range of superplasticity.

References

Balogh L., Ungár T., Zhao Y., Zhu Y.T., Horita Z., Xu C., Acta. Mater. 56 (2008) 809.

Furukawa M., Horita Z., Nemoto M., Valiev R.Z., Langdon T.G., Acta. Mater. 44 (1996) 4619.

Furukawa M., Horita Z., Nemoto M., Valiev R.Z., Langdon T.G., Philos. Mag. A 78 (1998) 203.

Furukawa M., Iwahashi Y., Horita Z., Nemoto M., Tsenev N.K., Valiev R.Z., Langdon T.G., Acta. Mater. 45 (1997) 4751.

Hall E.O., Proc. R. Soc. B. 64 (1951) 747.

Langdon T.G., Mater. Sci. 44 (2009) 5998

Loucif A., Figueiredo R.B., Baudin T., Brisset F., Langdon T.G., Mater. Sci. Eng. A 527 (2010) 4864.

Meyers M.A., Mishra A., Benson D.J., Prog. Mater. Sci. 51 (2006) 427.

Nurislamova *G., Sauvage X., Murashkin M., Islamgaliev R., Valiev R., Phil. Mag. Lett. 88 (**2008**) 459.*

Oh-Ishi *K., Horita Z., Smith D.J., Valiev R.Z., Nemoto M., Langdon T.G., Mater. Res. 14 (**1999**) 4200.*

Petch *N.J., Iron Steel Inst. 174 (**1953**) 25.*

Sergueeva *A.V., Stolyarov V.V., Valiev R.Z., Mukherjee A.K., Scripta Mater. 45 (**2001**) 747.*

Valiev *R.Z., Chmelik F., Bordeaux F., Kapelski G., Baudelet B., Scripta Metall. Mater. 27 (**1992**) 855.*

Zhang *H.W., Lu K., Pippan R., Huang X., Hansen N., Scripta Mater. 65 (**2011**) 481.*

Zhilyaev *A.P., Gimazov A.A., Soshnikova E.P., Révész Á., Langdon T.G., Mater. Sci. Eng. A 489 (**2008**) 207.*

Summary and Conclusion

An Al-0.6% Mg-0.4% Si alloy, in the form of disk with an initial grain size of about 150μm consistent and an average value of microhardness in the vicinity of about Hv=80 was used in this study. It has been successfully processed by HPT up to 20 complete revolutions at room temperature under pressure of 6 GPa using a rotation speed of 1 rpm after a solid solution treatment and aging at 423 K and 523 K. Based on the Vickers microhardness measurement and statistical information undertaken using EBSD and microtensile tests taken to record the microstructural and the mechanical properties evolution with increasing torsional straining conducted to several conclusions:

- Processing by HPT leads to an excellent grain refinement in the solution-treated condition with a reduction in grain size from 150 μm to 720 nm at the mid-radius of the disk in 1 turn of HPT processing and a further reduction to 250 nm after 20 turns surrounded by high fraction of high-angle grain boundaries of about 74%.
- The hardness increases significantly at the edge of the disk from Hv≈ 70 to Hv ≈ 142 after 1 turn in the periphery of the disc. After 10 and 20 turns the hardness tend to a saturation value (Hv ≈ 155) at equivalent strains above ~100.
- No significant change in the microstructures appears using processing at 100°C for the sample processed after 5 turns.
- For the aged conditions at 473 K and 523 K, the grain sizes are little larger than in the solid solution condition and achieved about 400 nm and 350 nm after 20 turns respectively. The fractions of HAGBs are quite similar in both conditions with ~74% of HAGBs in the solution-treated alloy and ~68% and ~76% in the aged conditions at 473 K and 523 K respectively.
- Observations based on orientation distribution function (ODF) calculation revealed an initial texture that was near random distribution and the development of an ideal torsion texture during HPT processing, often reported in the literature for fcc material. In particular, the C {001}<110> component was found to be dominant.
- No significant change in the texture sharpness was observed in this study with excessive deformation and this is attributed to the occurrence of dynamic recovery. Note also that

size (statistic) and positioning exact location as regard to the torsion experiments of scan areas may cause errors in the interpretation of textures.

- There is a deviation in the Hall–Petch relationship at grain sizes smaller than ~500 nm and this is consistent with an earlier suggestion that a breakdown may occur if there is an easy movement of the extrinsic dislocations in the non-equilibrium grain boundaries introduced by HPT processing.
- The mechanical testing at a temperature of 813 K gave similar stress-strain curves and no significant difference in the strength of the samples either after solid solution and aging conditions. Aging at 523 K leads to the maximum recorded elongations to failure of ~230% which is not within the range of superplasticity.

References

B

Balogh L., Ungár T., Zhao Y., Zhu Y.T., Horita Z., Xu C., Acta. Mater. 56 (2008) 809.

Bay B., Hansen N., Hughes D.A, Kulhmann-Willsdorf D., Acta Metall. & Mater. 40 (1992) 205

Beausir B., Tóth L.S., Neale K.W. Acta Mater. 55 (2007) 2695-2705.

Bridgman P.W., Appl. Phys. 14 (1943) 273.

Bunge H.J., Texture Analysis in Materials Science, Butterworth, London (1982).

Bunge H.J., Z. Metallkd. 56 (1965) 872.

C

Cayron C., Sagalowicz L., Beffort O., Buffat P. A., Phil. Mag. 79 (11) (1999) 2833- 2851.

Chakrabarti D. J, Laughlin D. E., Progress Mater. Sci. 49 (2004) 389-410.

D

Dimier F., Ph.D thesis, Superior National School of Mines. Paris (2003).

Dobatkin S.V., Bastarache E.N., Sakai G., Fujita T., Horita Z., Langdon T.G., Mater Sci Eng A 408 (2005) 141.

Dobatkin S.V., Zhu Y.T., Langdon T.G., Mishra R.S., Semiatin S.L., Saran M.J., Lowe T.C., editors. Ultrafine grained materials II. Warrendale, PA: The Minerals, Metals and Materials Society;(2002) 183.

Doherty R.D., Hughes D.A., Humphreys F.J., Mater. Sci. Eng. A238 (1997) 219.

E

Edalati K., Fujioka T., Horita Z. Mater. Sci. Eng. A 497 (2009) 168.

Esmaeili S., Wang X., Lloyd D. J., Poole W. J., Met. Mater. Trans. 34(A) (2003) 751-762.

Estrin Y., Molotnikov A., Davies C.H.J., Lapovok R., Mech J., Phys. Solids 56 (2008) 1186.

F

Furukawa M., Horita Z., Langdon T.G., Metals Mater 9 (2003) 141.

Furukawa M., Horita Z., Nemoto M., Valiev R.Z., Langdon T.G., Acta Mater. 44 (1996) 4619.

Furukawa M., Horita Z., Nemoto M., Valiev R.Z., Langdon T.G., Phil. Mag. A 78 (1998) 203.

Furukawa M., Iwahashi Y., Horita Z., Nemoto M., Tsenev N.K., Valiev R.Z., Langdon T.G., Acta Mater. 45 (1997) 4751.

G

Germain L., Ph.D thesis, Paul Verlaine Metz University (2006)

Gomes R. M., Sato T., Tezuka H., Kamio A,. Mater. Trans JIM. 39(3) (1998) 353-364.

H

Hall E.O., Proc. R. Soc. B 64(1951) 747.

Hansen J., Pospiech J., Lücke K., Tables for Textures Analysis of Cubic Metals, Springer Verlag Berlin, Heidelberg New-York, (1978).

Hansen N., Scripta Metall. and Mater. 27 (1992) 1447.

Harai Y., Ito Y., Horita Z. Scripta Mater. 58 (2008) 469.

Hirth S. M., Marshall G. J., S. A. Court, D. J. Lloyd, Mater. Sci. Eng. A 329-321 (2001) 452-456.

Horita Z., Furukawa M., Nemoto M., Langdon T. G. Mater Sci Tech 16 (2000) 1239.

Horita Z., Smith D.J., Furukawa M., Nemoto M., Valiev R.Z., Langdon T.G., Mater Res 11(1996) 1880

Hughes D.A., Hansen N., Mater. Sci. Tech. 7 (1991) 544.

Hughes D.A., Proceedings of the Sixteenth Risø International Symposium on Material Science, Edited by N. Hansen, D. Juul Jensen, Y.L. Liu, B. Ralph, Roskilde, Denmark (2000) 63.

I

Islamgaliev R.K., Yunusova N.F., Sabirov I.N., Sergueeva A.V., Valiev R.Z., Mater. Sc.i Eng. A 877(2001) 319–321.

Iwahashi Y., Wang J., Horita Z., Nemoto M., Langdon T.G. Scripta Mater (1996) 35-143.

Ito Y., Horita Z., Mater. Sci. Eng. A 503 (2009) 32.

K

Kawasaki M., Langdona T. G., Mater. Sci. Eng. A 528 (2011) 6140–6145.

Kawasaki M., Ahn B., Langdon T.G., Acta Mater. 58 (2010) 919.

Kawasaki M., Horita Z., Langdon T.G., Mater. Sci. Eng. A524 (2009) 143.

Komura S., Horita Z., Furukawa M., Nemoto M., Langdon T.G., Metall. Mater. Trans. A 32 (2001) 707.

Krallics G., Lenard J. G., J. Mater.Proc.Tech. (2004) 152-154.

L

Langdon T.G., Mater. Sci. 44 (2009) 5998

Li S., Beyerlein I.J., Bourke M.A., Mater. Sci. Eng. A 394 (2005) 66-77.

Loucif A., Figueiredo R.B., Baudin T., Brisset F., Langdon T.G., Mater. Sci. Eng. A 527 (2010) 4864.

Lück K., Pospiech J., Virnich K.H., Jura J., Acta Metall. 29 (1981)167-185.

M

Mackenzie J.K., Biometrika 45 (1958) 229.

Marioara C. D., Ph.D Thesis, Norwegian University of Science and Technology (NTNU) (2000).

Megumi K., Terence G. L., Mater. Sci. Eng A 528 (2011) 6140–6145.

Meyers M.A., Mishra A., Benson D, Prog. Mater. Sci 46 (2005) 443.

Meyers M.A., Mishra A., Benson D.J., Prog. Mater. Sci. 51 (2006) 427.

Miao W. F., Laughlin D. E., Met. Mater. Trans. 31 (2000) 361-371.

Mishra R.S., Valiev R.Z., McFadden S.X., Islamgaliev R.K., Mukherjee A.K., Philos Mag A 81 (2001)37.

Montheillet F., Cohen M., Jonas J.J., Acta Metall. 32 (1984) 2077.

N

Nemoto M., Horita Z., Furukawa M., Langdon T. G., Meta. Mater. 4 (1998) 1181

Nurislamova G., Sauvage X., Murashkin M., Islamgaliev R., Valiev R., Phil. Mag. Lett. 88 (2008) 459.

O

Oh-Ishi K., Horita Z., Smith D.J., Valiev R.Z., Nemoto M., Langdon T.G., Mater. Res. 14 (1999) 4200.

Ohmori Y., Doan L. C., Nakai K. Mater. Trans. 43(2002) 246-255.

Orlov D., Bhattacharjee P. P., Todaka Y., Umemoto M., Tsuji N., Scripta Mater 60 (2009) 893.

P

Petch N.J., J Iron Steel Inst 174 (1953) 25.

Pippan R., Scheriau S., Taylor A., Hafok M., Hohenwarter A, Bachmaier A., Ann. Rev. Mater. Res. 40 (2010) 319.

Pippan R., Wetscher F., Hafok M., Vorhauer A., Sabirov I., Adv. Eng. Mater. 8 (2006) 1046.

R

Randle V., Engler O., Introduction to texture analysis. Macrotexture, microtexture & orientation mapping. Gordon and Breach Science Publishers (2000).

Roe R. J., Appl. Phys. 36 (1965) 4329.

S

Sakai G., Horita Z., Langdon T.G., Mater. Sci. Eng. A 393 (2005a) 344.

Sakai G., Nakamura K., Horita Z., Langdon T.G. Mater Sci Eng A 406 (2005b) 268.

Saito Y., Utsunomiya H., Tsuji N., Sahai T. Acta mater 47 (1999) 579-583.

Senkov O.N., Froes F.H., Stolyarov V.V., Valiev R.Z., Liu J. Nanostruct Mater 10 (1998) 691.

Sergueeva A.V., Stolyarov V.V., Valiev R.Z., Mukherjee A.K., Scripta Mater. 45 (2001) 747.

Serre P, Figueiredo R.B, Gao N, Langdon T.G., Mater Sci Eng A 528 (2011) 3601

Skinner D. J., Bye R. L., Raybould D., Scripta Met. 20 (1986) 867-872.

Straumal B.B., Baretzky B., Mazilkin A.A., Phillipp F., Kogtenkova O.A., Volkov M.N. Acta Mater 52 (2004)4469.

T

Tóth L.S., Massion R.A., Germain L., Baik S.C., Suwas S., Acta Mater 52 (2004) 1885.

Tóth L.S., Neal K.W., Jonas J.J., Acta. Metal.l 37 (1989) 2197.

Troger L.P., Starke E.F., Mater. Sci. Eng. A 277 (2000) 102-113.

V

Valiev R.Z., Chmelik F., Bordeaux F., Kapelski G., Baudelet B., Scripta Metall. Mater. 27 (1992) 855.

Valiev R.Z., Ivanisenko Yu.V., Rauch E.F., Baudelet B., Acta. Mater. 44 (1996) 4705.

Valiev R. Z., Langdon T.G., Prog. Mater. Sci. (2006) 881-981.

Valiev R.Z., Zehetbauer M.J., Estrin Y., Höppel H.W., Ivanisenko Y., Hahn H., Adv. Eng. Mater. 9 (2007) 527.

Virnich H.J., Pospiech J., Flemmer A., Luck K., Proc ICOTOM 5, Aachen, March (1978).

Vorhauer A., Pippan R., Scripta Mater. 51 (2004) 921.

W

Wagner F., PhD thesis, Metz University (1983).

Wang X., Poole W. J., Esmaeili S., Lloyd D. J. Embury J. D., Met. Mater. Trans. 34(A) (2003) 2913-2918.

Wetscher F., Vorhauer A., Stock R., Pippan R., Mater. Sci. Eng. A 809 (2004) 387–389.

X

Xu C., Horita Z., Langdon T.G., Acta. Mater. 55(2007)203.

Xu C., Horita Z, Langdon T.G., Acta Mater. 56 (2008a) 5168.

Xu C., Horita Z., Langdon T.G., Mater. Sci. 43 (2008b) 7286.

Xu C., Langdon T.G., Scripta Mater. 48 (2003) 1.

Xu C., Langdon T.G., Mater. Sci. Eng. A 503 (2009) 71.

Xu C., Horita Z., Langdon T.G., Mater. Sci. Eng. A528 (2011) 6059.

Xu C., Horita Z., Langdon T.G., Mater. Trans. 51 (2010) 2.

Z

Zhang H.W., Lu K., Pippan R., Huang X., Hansen N., Scripta Mater. 65 (2011) 481.

Zheng J. G., Vincent R., Steeds J. W., Phil. Mag. 80 (A) (2000) 493-500.

Zhilyaev A.P.,Lee S., Nurislamova G.V., Valiev R.Z., Langdon T.G., Scripta Mater 4 (2001) 2753.

Zhilyaev A.P., Kim B.K., Nurislamova G.V., Baró M.D., Szpunar J.A.,Langdon T.G, Scripta Mater. 46 (2002) 575.

Zhilyaev A.P., Nurislamova G.V., Kim B.K., Baró M.D., Szpunar J.A., Langdon T.G., Acta Mater 51 (2003) 753.

Zhilyaev A. P., Baró M. D., Langdon T. G., McNelley T. R., Rev Adv Mater Sci. 7 (2004) 41.168 Textures of Materials

Zhilyaev A.P., Kim B.K., Szpunar J.A., Baró M.D., Langdon T.G, Mater. Sci. Eng. A 391 (2005) 377.

Zhilyaev A.P., Oh-ishi K., Raab G.I., McNelley T.R., Mater. Sci. Eng., A 441 (2006a) 245.

Zhilyaev A.P., Swisher D.L., Oh-ishi K., Langdon T.G., McNelley T.R., Mater. Sci. Eng. A 429 (2006b) 137.

Zhilyaev A.P., McNelley T.R.,. Langdon T.G, Mater. Sci. 42 (2007) 1517.

Zhilyaev A.P., Langdon T.G., Prog. Mater. Sci., 53 (2008) 893-979.

Zhilyaev AP, Gimazov AA, Soshnikova EP, Révész Á, Langdon TG., Mater Sci Eng A 2008;489:207.